Renewable and Sustainable Energy Reviews 30 (2014) 195–216

Contents lists available at ScienceDirect

Renewable and Sustainable Energy Reviews

journal homepage: www.elsevier.com/locate/rser

Progress in combustion investigations of hydrogen enriched hydrocarbons

Chenglong Tang, Yingjia Zhang, Zuohua Huang *

State Key Laboratory of Multiphase Flows in Power Engineering, Xi'an Jiaotong University, Xi'an 710049, People's Republic of China

ARTICLE INFO

Article history:
Received 23 July 2013
Received in revised form
12 September 2013
Accepted 13 October 2013
Available online 5 November 2013

Key words:
Hydrogen enriched combustion
Ignition delay time
Laminar flame speed
Flame front stability
Pollutant emission

ABSTRACT

Due to industrial development and population growth, global demand for energy has increased enormously; the increased consumption of primary sources of energy such as coal, oil and natural gas has exerted a strong influence on the atmospheric environment. Among all the alternative fuels, hydrogen offers the greatest potential benefits to energy supply and the environment. However, combustion of pure hydrogen is challenged by the difficulties in production, storage, and end-use. A more reasonable method to enhance combustion is to use hydrogen as an additive to fossil fuels.

This paper presents a comprehensive review of recent progress in fundamental investigations of hydrogen enriched combustion. A broad range of topics on fundamental combustion of hydrogen/hydrocarbon mixtures are discussed. The minimum ignition energy of hydrogen/hydrocarbon blends shows significant decrease with the increased hydrogen fraction X_{H2}. With an increase of the hydrogen fraction, ignition behavior of hydrogen/hydrocarbon fuel blends exhibits three distinct behaviors. Additionally, the laminar flame speed of hydrogen/hydrocarbon fuel blends is found to exhibit three behavior regimes. Furthermore, the flame front instability behavior is influenced by the hydrogen addition through the combined effect of body force, the hydrodynamic effect and the thermal-diffusion effect.

Contents

* Corresponding author. Tel.: +86 29 82665075; fax: +86 29 82668789.
E-mail address: zhhuang@mail.xjtu.edu.cn (Z. Huang).

1364-0321/$ - see front matter
http://dx.doi.org/10.1016/j.rser.2013.10.005

1. Introduction

Fossil fuels in the form of coal, oil, and natural gas have been used in transportation, heating, and power plants since the beginning of the industrial revolution in the 18th century. However, increasing global demand for energy due to industrial development and population growth is being threatened by the limited supply of fossil fuel. Additionally, the fact that oil is found primarily in only a few regions of the world creates a strong economic dependence, especially in developing countries. Furthermore, the combustion of fossil fuel produces carbon dioxide, which has been named as a primary cause of global warming; and the chemical and particulate emissions produced from burning of fossil fuel put human health at risk.

1.1. The status of hydrogen technology: production, storage, and end-use

Research on alternative fuels have been driven by environmental and energy supply challenges. Among the various alternative fuels, hydrogen offers the significant potential benefits to the environment and energy supply [1]. Hydrogen is the most abundant element on Earth, but only 1% exists in the form of molecular hydrogen H_2. There are a variety of widely available methods for producing hydrogen. Currently, commercially available hydrogen is primarily produced through steam reforming from natural gas, in which carbon-fuel is still used [2].

Cost effective ways to mass produce hydrogen from non-carbon fuel is a challenge to the use of hydrogen as a substitute for fossil fuels. The most promising method is splitting water. However, it takes energy to split water molecule, even though that energy is later replaced by energy released from the oxidation of hydrogen [3]. Non-carbon sources of energy such as solar, nuclear, hydroelectric, or wind energies have been tested in the water-splitting process, the goal being to eliminate fossil fuels from the water-splitting cycle.

Regarding the issue of on-board storage, a US Department of Energy (DOE), Hydrogen Program has set a standard [4]: the storage system should contain a hydrogen weight of at least 6.5% of the system weight, and the volumetric density of 62 kg H_2/m^3. Conventionally, hydrogen is stored in a high pressure steel tank, with a typical filled pressure of up to 200 bar in most countries. Carbon/polymer tanks, or fiberglass/aluminum tanks, can withstand pressures as high as 600 bar, but the volumetric energy density is still low. Storage of H_2 on activated carbon (AC) materials at temperatures below 150 K has been investigated and proved unsatisfactory [5]. Liquefied hydrogen has better volumetric energy density, but the process of liquefaction requires large amounts of energy to create an environment with temperatures as low as 20 K and perfect insulation techniques. Some metals or alloys can form hydrides, which can release hydrogen, but the gravimetric density is typically less than 3% due to the heaviness of the metals. Single-walled carbon nanotubes (SWNTs) can absorb large amounts of hydrogen into its molecularly dimensioned pores. Fig. 1 shows that none of the hydrogen storage techniques is capable of meeting DOE goals [6], but there is reason to expect that one day better hydrogen storage materials and techniques will be discovered and developed.

There are essentially two methods for hydrogen usage: hydrogen fuel cells and hydrogen internal combustion engines. A fuel cell converts the chemical energy of the fuel directly to electricity. A hydrogen–oxygen fuel cell has an ideal electrical conversion efficiency of 83%. In a real fuel cell, up to 60% of the chemical energy is converted to electricity, and the remainder is converted to heat. Theoretically many other fuels can be used in fuel cells, but hydrogen is the best candidate because of the rapid reaction kinetics at the anode. Worldwide efforts have been made to commercialize the proton exchange membrane (PEM), fuel cell in the last few years; however, the cost of PEM fuel cells is still much higher than conventional internal combustion engines. The cost of power for PEMs fuel cells for transportation is \$1500–10,000 per kilowatt, while the power cost of conventional automobile is less than \$50 per kilowatt [3].

1.2. Hydrogen as an enriching agent

Lean combustion of hydrocarbon in nearly all combustors such as gas turbines, furnaces, boilers and internal combustion engines

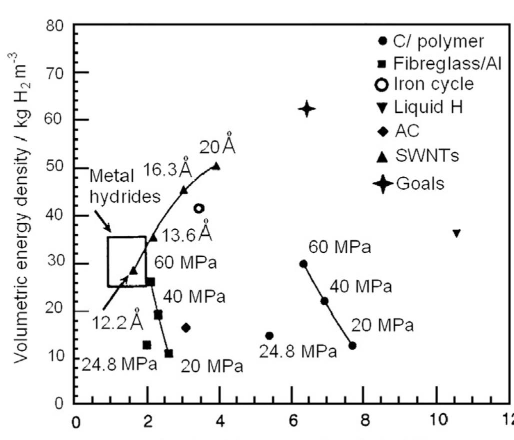


Fig. 1. Installed energy densities for several vehicular hydrogen storage techniques, from Ref. [6].

Nomenclature

ϕ	equivalence ratio
σ	thermo expansion rati
κ	stretch rate
E_a	activation energy
$E_{I,min}$	minimum ignition energy
Ka	Karlovitz number
p	pressure
R_H	hydrogen addition parameter, see Eq. (11)
T	temperature
U	internal energy
X_{H2}	hydrogen fraction in the fuel blends
ϕ_F	Fuel based equivalence ratio, see Eq. (10)
κ_{ext}	extinction strain rate
d_q	quenching distance
k	linearity coefficient, see Eq. (13)
f	mass burning flux
Le	Lewis number
r_f	flame radius
S_u^0	laminar flame speed T_u unburned gas temperature
T_{ad}	adiabatic flame temperature
V	volume
Ze	Zeldovich number

Abbreviations

CCMHDI	combustion chemistry of methane and hydrogen dominated ignition
HCDI	hydrogen chemistry dominated ignition
LPC	lean premixed combustion
MIE	minimum ignition energy
PR	pressure rise
UFL	upper flammability limit
HCNG	hydrogen/compressed natural gas
LFL	lower flammability limit
MCDI	methane chemistry dominated ignition
NG	natural gas
SFHC	stoichiometric fraction of the hydrocarbon in the fuel mixtures
VI	visualization

is advantageous in terms of NO_x, CO and unburned HC emissions as well as for fuel economy. However, lean hydrocarbon/air mixtures are hard to ignite and have low flame speed, which can potentially cause misfire and results in increased unburned hydrocarbons, reduced performance and poor fuel economy. In addition, lean hydrocarbon flame is hard to burn steadily, which causes malfunction of the combustors.

The properties that contribute to use of hydrogen in internal combustion engines are its wide flammability range, which enables hydrogen to run on a very lean mixture; low ignition energy, which ensures prompt ignition; high reactivity and flame speed, which moves the real engine cycle closer to the thermodynamic ideal; high diffusivity, which facilitates the uniformity of fuel and air; and high auto-ignition temperature, which allows larger compression ratio of the engine. However, when pure hydrogen is used, the engines are prone to pre-ignition due to hydrogen's lower ignition energy, wider flammability range and shorter quenching distance. In addition, when pure hydrogen is burned in the engine, the heat release is very fast, and the temperature is high; thus the engine could potentially emit high levels of NO_x and engine reliability is challenged because of the high thermal load.

To some extent the drawbacks of burning pure hydrogen or pure hydrocarbons can be reduced simultaneously by mixing hydrocarbon with a certain amount of hydrogen. The low ignition energy of hydrogen makes hydrogen/hydrocarbon mixtures easier to ignite. Hydrogen's high flame speed reduces misfire, thereby reducing emissions. The energy density of the mixture is augmented because of the increased hydrogen-to-carbon ratio; thus the torque is improved at wide open throttle conditions. Using hydrogen as a hydrocarbon combustion stimulant has received considerable attention as a near term solution, before a full hydrogen infrastructure – in terms of production, storage and end-use – is established.

1.3. Outline of the review

Following is a review of the wide spectrum of research activities on hydrogen stimulated hydrocarbon combustion. I In Section 2, the flammability limits of hydrogen enriched hydrocarbons are discussed. In Section 3, the literature on the effect of hydrogen addition on spark ignition characteristics is presented, followed by a discussion on the hydrogen addition effect on auto-ignition by shock waves, in Section 4. The hydrogen addition effects on laminar flame speed and flame front instability of hydrocarbon/air mixture are reviewed in Section 5. In Section 6, the hydrogen addition effect on lean premixed combustion stability and emissions from lean premixed combustion is reviewed.

2. Flammability limits

A lower flammability limit (*LFL*) and an upper flammability limit (*UFL*) are typically determined for a fuel–oxidizer system at a given pressure and temperature, and when the fuel/oxidizer ratio is lower than *LFL*, or higher than *UFL*, the mixture is inflammable. The studies on flammability issues are primarily motivated by its importance in assessing fire hazards. In addition, advantages in lean combustion, such as improved emissions and efficiency characteristics, are limited by the *LFL*.

2.1. Flammability limits of hydrocarbons

There are several experimental techniques which determine flammability limits. The most direct and best known method is the so-called visual identification method (VI), developed by the former US Bureau of Mines. In this method, the mixture is defined as "flammable" if the flame, induced by a spark at the bottom of a vertically oriented glass tube, can propagate upwardly a certain distance. Much of the work with this method was performed and summarized by Coward and Jones [7], Zabetakis [8], and Kuchta [9]. Table 1 shows some examples of the flammability limits, determined using the visual identification (VI) method. It is seen that hydrogen has the lowest *LFL*, indicating that hydrogen is potentially capable of burning under very lean mixture conditions.

Another apparatus for measuring the flammability limit is a closed, spherical reaction vessel with central ignition. In this method, the flammability criterion is the relative pressure increase from combustion. The Pittsburgh Research Laboratory has published considerable flammability data using the pressure rise (PR) criterion [10–12]. A counter-flow burner can also be used to determine the flammability limit. In this method, the global strain rate (a gradient of

Table 1
Flammability limits of some common fuels at 1 atm, 25 °C. Data from Ref. [8].

Fuel	ϕ	
	LFL	UFL
Hydrogen	0.1	7.14
Carbon monoxide	0.34	6.8
Ammonia	0.63	1.4
Methane	0.5	1.67
Ethane	0.52	2.4
Propane	0.56	2.7
Butane	0.57	2.8
Ethylene	0.40	8.0
Acetylene	0.31	∞
Benzene	0.56	3.7
Methanol	0.51	4.0
Ethanol	0.41	2.8

the exit velocity) is plotted as a function of fuel concentration. The flammability limit can be obtained by extrapolating the curve to the minimum strain rate [13].

Various organizations have attempted to standardize the measurements of flammability limits. To list some examples: The American Society for Testing and Materials (ASTM) has used a 5 L glass sphere (ASTM E681), to visually detect the flame propagation in order to define the flammability [14], a 4 L near-spherical vessel (ASTM E2079), with high ignition energy and the 7% pressure rise criterion [15], and a 1 L minimum vessel with 76 mm diameter (ASTM E918), with 7% pressure rise criterion, capable of operating under elevated temperatures and pressures [16]. The European Standard EN 1839 is subdivided into EN 1839T and EN 1839B. EN 1839T defines flammability by detecting 10 cm of flame propagation upon ignition in a glass cylinder, and the EN 1839B uses the 5% pressure increase in a cylinder or spherical vessel with volume larger than 5 L. ISO 10156 recommended ASTM E181 and EN 1839T as the experimental criteria for flammability determination. Van den Schoor et al. [17] and Schröder and Daubitz [18] compared EN and ASTM methods and their investigation showed similar results for the most important gases and gas mixtures.

Increasing computational capability and development of reaction mechanisms makes possible the numerical simulation of limited flames with different geometries. Simulation attempts include 1D planar flame [19,20] and the quasi-1D spherically propagating flame [21], with or without radiation heat loss. Theoretically, there exists a limiting flame speed below which the flame is unable to propagate; this approach had been used to determine flammability limits [22,23]. Analogous to the limiting flame speed approach, Burgess and Wheeler [24] proposed a temperature limiting concept, which states that for many lean limit hydrocarbons–air mixtures, the *LFL* (in terms of fuel volume fraction) times the heating value of the fuel, $q_{c,i}$, is nearly a constant around 920 kcal/mole, limiting the temperature to around 1450 K [25,26]. This concept is implicitly used when applying Le Chatelier's mixing rule, which is based on the assumption that the heat of combustion of the mixture at the lean flammability limit is the heat of combustion of its composing fuels at their respective *LFL*s, as shown in the following equation:

$$(LFL)_{mix} = \left[\sum_{i=1}^{n} \frac{X_i}{(LFL)_i} \right]^{-1} \tag{1}$$

where X_i is the volume fraction of the fuel i and $(LFL)_i$ is its corresponding flammability limit, and n is the total number of fuel components.

2.2. Flammability limit of hydrogen/hydrocarbon mixtures

Several researchers have tested the effects of hydrogen addition on the flammability limits of premixed hydrocarbon air mixtures with a variety of methods described in Section 2.1. Wierzba and Ale [27] investigated the effect of hydrogen addition on the rich flammability limit of methane, ethylene, and propane at elevated temperatures with the VI method. Their measured *UFL* significantly increases when hydrogen is added, and for methane and propane the measurements agree well, but for ethylene the results deviate remarkably with the predictions by Le Chatelier's Rule. Shoshin and de Goey [28] also measured the flammability limit of methane/hydrogen/air mixtures with the VI method – especially the effects of tube diameter. Miao et al. [29] measured the flammability limit of natural gas/H_2 and methane/H_2 blends using the PR method; their results showed no difference between natural gas and methane. In Ref. [17], Van den Schoor et al. applied the VI and PR method, as well as a planar and spherical flame model to a methane/hydrogen/air system; the limiting burning velocity of 5 cm/s criterion predicts the *UFL* well, as compared with the experimental results. Guo et al. [30] studied the hydrogen addition effect on the flammability limit of an ultra-lean methane/air stream. As shown in Fig. 2, the upper branch is the stretch extinction limit, caused by high stretch rate, and the lower branch is the radiation extinction limit, due to an ultra low stretch rate. It is seen that with the increase of X_{H2}, both limits shift to a leaner mixture, thus the turning point of the "C" shaped curve, defined as the *LFL*, is consequently decreased.

The recent literature reporting flammability limit data of hydrogen/methane/air mixtures was summarized in a flammability regime diagram in the parameter space of hydrogen fraction X_{H2} and equivalence ratio ϕ, as shown in Fig. 3. The flammable and nonflammable regimes are separated by the *LFL* and *UFL*. The experimentally measured *LFL*s with different techniques are consistent. For the *UFL*s, large discrepancies exist among different literatures. The predictions by Le Chatelier's Rule were also shown in Fig. 3; data of *LFL* and *UFL* of methane and hydrogen in Table 1 were used. For *LFL*, Le Chatelier's prediction is in good agreement with those measurements, but for *UFL*, the prediction deviated considerably from most of the experimental measured results.

3. Hydrogen assisted ignition

The flame is initiated through two methods: one is forced ignition by an electric spark, laser, hot air jets or plasma; the other is auto-ignition by shock waves, which will be discussed in Section 4.

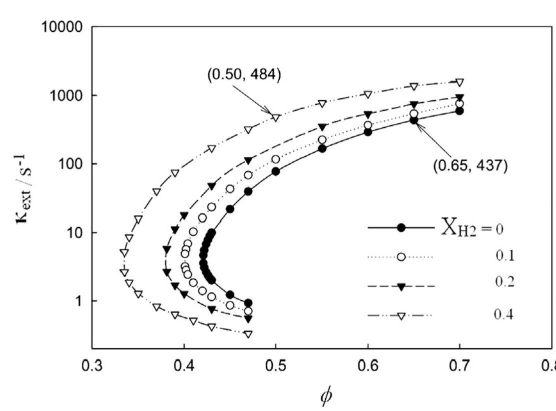


Fig. 2. Extinction strain rate as a function of equivalence ratio for counter-flowing methane/hydrogen/air mixtures [30].

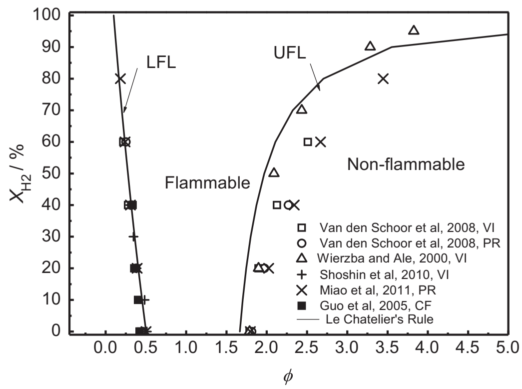


Fig. 3. Flammability region diagram for methane/hydrogen/air mixture at 1 atm and room temperature [17,27–30].

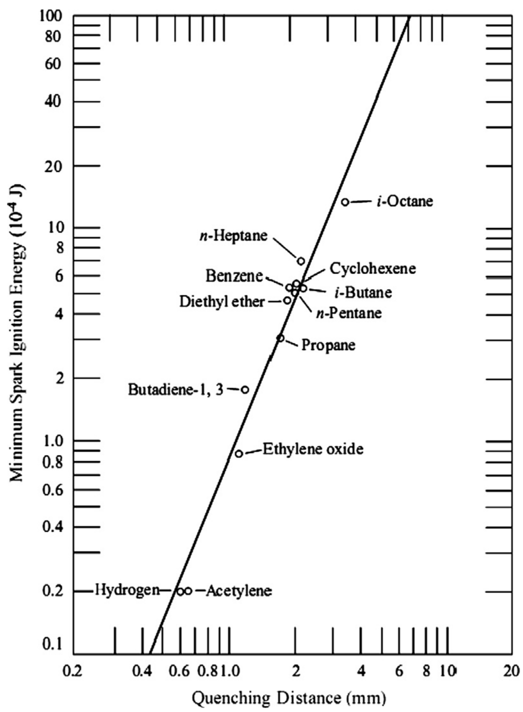


Fig. 4. Correlation of the MIEs with quenching diameter for different fuels. Adapted from Calcote et al. [33].

3.1. Spark ignition of premixed hydrogen/hydrocarbon/air mixtures

3.1.1. Thermal-diffusion theory on MIE

Generally, ignition of combustible mixture is initiated by an electric spark, and the subsequent flame is propagated outward in an expanding sphere. The literatures show that the spark ignition progresses in three stages: the breakdown stage, the arc stage and the glow stage. The breakdown stage occurs in a timescale of 10^{-6} s, during which a conducting channel, consisting of high temperature equilibrium plasma, is opened. In the subsequent arc stage, the plasma kernel grows due to the deposit of electric energy. The last stage is the ignition of the combustion mixture surrounding the hot plasma kernel. The overall energy deposit by the spark is the most important factor for successful ignition. Minimum ignition energy (MIE) is the minimum energy required to ignite a combustible mixture. In the thermal-diffusion theory [31,32], MIE has been constantly correlated to the quenching distance, d_q, or laminar flame thickness, δ_l. For fuels with different molecular structures, Calcote et al. [33] have correlated their MIEs, $E_{I,min}$, with the measured d_q as shown in Fig. 4. The slope of the line in the logarithmic scale yields the following relation:

$$E_{I,\,min} \sim d_q^{2.48} \quad (2)$$

Williams [32] also empirically correlated, and a power of 2 was proposed. Glassman [34] and Law [25] stated that MIE should be proportional to the amount of energy needed to heat a spherical volume of the mixture of radius of the order of laminar flame thickness, δ_l (of the order of quenching distance), to the burned temperature (close to T_{ad}), yielding

$$E_{I,\,min} \sim \rho_u \delta_l^3 c_P (T_{ad} - T_u) \sim d_q^3 \quad (3)$$

To the authors' knowledge, the only literature which reports on the minimum ignition energy and quenching distance for hydrogen/methane/air mixture is by Hankinson et al. [35] and Fukuda et al. [36]. The minimum ignition energy and the quenching distance both decrease with the increase of X_{H2}, indicating that the addition of hydrogen is potentially capable of facilitating successful ignition.

$E_{I,min}$ and d_q for methane/hydrogen/air mixtures were correlated in Fig. 5 for hydrogen fractions of 0, 25%, 50%, 75% and 100%. The data were obtained directly or through interpolation from Refs. [35,36]. It is seen that $E_{I,min}$ and dq for all mixture conditions could be linearly correlated in the logarithmic scale, yielding

$$E_{I,\,min} \sim d_q^{2.32} \quad (4)$$

in which the power of 2.32 compares favorably with that determined by Calcote et al. [33]. Eqs. (2) and (4) are obtained by fitting the experimental data, while Eq. (3) is derived based on the

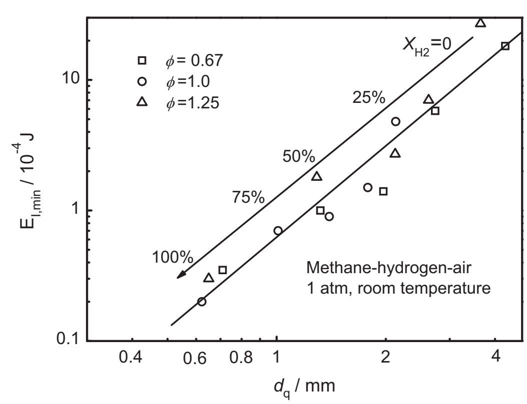


Fig. 5. Minimum ignition energy as a function of quenching distance for methane/hydrogen/air mixture at 1 atm and room temperature. Data obtained from Refs. [35,36].

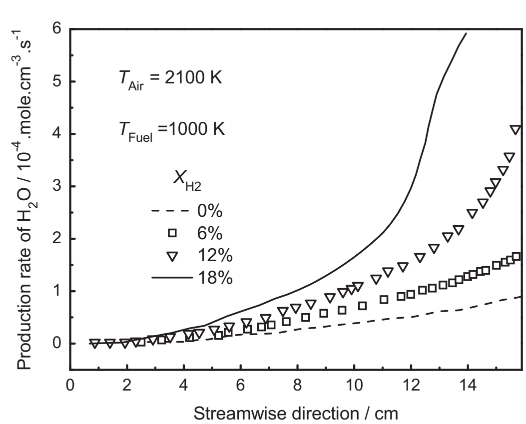


Fig. 6. Rate of production of H_2O profile for $X_{H2} < 20\%$. Adapted from Ju and Niioka [45].

thermal-diffusion theory and the level of agreement between the experimental measurement and theoretical prediction is acceptable.

3.1.2. Self-sustained flame propagation

The minimum ignition energy has been extensively measured [31,33], based on which ignition process is better realized; however, the flame dynamics at the initial stage were not included in these studies. Because the flame kernel radius was very small, the stretch effect could be large, and could possibly result in failure to form flame propagation. Law [25] proposed a generalized factor to quantify the transient effect of stretch

$$\sigma = \frac{Ze}{2}(Le^{-1}-1)Ka \tag{5}$$

where

$$Ze = \frac{E_a(T_{ad}-T_u)}{R^0T_{ad}^2}, \quad Ka = \frac{\delta_l}{s_u^0}\kappa \quad \text{and} \quad \kappa = \frac{2}{r_f}\frac{dr_f}{dt}$$

are respectively the Zeldovich number, Karlovitz number and the instantaneous stretch for outwardly propagating flames. Furthermore, Le, E_a, T_{ad}, T_u, R^0, $s_u{}^0$ and r_f are respectively the Lewis number, activation energy, adiabatic temperature, unburned gas temperature, universal gas constant, laminar flame speed and flame radius.

It is noted that the Karlovitz number, which demonstrates the effect of stretch, and the Lewis number, which represents the effect of non-equidiffusion, are intrinsically coupled, and Ze represents the chemical weighing in Eq. (5). In addition, outwardly propagating spherical flame experiences positive stretch. Eq. (5) shows that the temperature (hence the flame propagation) is promoted if $Le<1$, while the opposite holds for $Le>1$. In the latter case, the competition between the electric energy supply and the stretch effect may result in failure of a self-sustained propagating flame if the flame radius does not grow large enough beyond which the stretch effect could be negligible.

Recently, He [37] and Chen and Ju [38], numerically investigated the propagation of spherical flames, allowing for continuous supply of ignition energy. The results showed that for $Le<1$ mixture, the initial high flame speed due to spark energy supply decreases to planar value as the flame expands (provided that a flame kernel is successfully established). While for $Le>1$ mixture, the response is quite different. If the ignition energy is sufficiently large, the flame speed decreases to a minimum value and then increases to the planar value. Otherwise, the continuously decelerating flame will extinguish at a certain flame radius. Kelley et al. [39] then experimentally examined the above theoretical predictions with hydrogen/air and butane/air flames. Indeed, the flame propagation behavior for lean hydrogen/air mixture and rich butane/air mixture ($Le<1$) is quite similar, so that the flame propagation speed decreases to an asymptotic value. However, for the case of very rich hydrogen/air or lean butane/air mixture ($Le>1$), the flame speed first decreases to a minimum, and the self-sustained flame propagation is subsequently recovered.

Although there have been no publications about flame kernel growth for a hydrogen/hydrocarbon/air mixture, it is anticipated that adding hydrogen to a lean hydrocarbon/air mixture will influence the flame kernel evolution, because hydrogen will affect the preferential diffusion characteristics of hydrocarbons–air mixture, as will be discussed in detail in Section 5.2.

3.2. Ignition of methane/hydrogen and air in supersonic mixing layer

The practical objective of the studies on ignition in supersonic mixing layers is the determination of ignition distance in response to the interest in the development of scramjet engines. The ignition kinetics of hydrogen/air [40,41] and methane/air [42] has been studied and methane was found to have a long ignition delay time. Thus ignition improvement is required. Silane is an effective candidate, but its highly reactive nature renders on-board use difficult and dangerous [43]. Hence hydrogen could be more practically used as the ignition stimulus. For instance, Bier et al. [44] conducted experiments on the ignition of transversely injected methane and hydrogen into parallel supersonic air stream and found that the lowest static air temperature for stable combustion of hydrogen was 700 °C – much lower than 1300 °C – which is the corresponding value for methane. However, there have been only a few investigations on the ignition of methane/hydrogen vs. air stream in supersonic mixing layer. Ju and Niioka [45] numerically investigated the effect of hydrogen fraction in the methane/hydrogen fuel stream (here, also designated as X_{H2}) on the ignition process. Velocities of the air and fuel mixture streams were set to be 1200 and 1000 m/s, respectively. The computational domain is 16×3 cm^2. They found that the ignition behavior strongly depends on X_{H2}. As shown in Fig. 6, for X_{H2} less than 9% (although strong ignition was not observed in the computational domain), the concentration of the produced H_2O still increased with increasing X_{H2}. When X_{H2} was further increased up to 12%, a sharp increase in the rate of production of H_2O was observed in the computational domain, which is the manifestation of strong ignition.

For a very high hydrogen fraction up to 85%, the mixture behaves analogously to hydrogen and the presence of methane acts as an ignition inhibitor. Ju and Niioka [45] identified three sub-regimes with increasing methane fraction X_{CH4} (decreasing X_{H2}). As shown in Fig. 7, in the first sub-regime, the presence of even a very small amount of methane significantly increased the ignition distance. This significant increase leveled off in the second sub-regime. In the third sub-regime as methane concentration was further increased, a second rapid increase in ignition time was observed. Specifically, for $X_{CH4}<2\%$, the ignition time increased quickly with increasing X_{CH4}. In this sub-regime, the endothermic reaction $CH_4 \leftrightarrow CH_3 + H$ and the H radical scavenging reaction $H + CH_4 \leftrightarrow CH_3 + H_2$ were both promoted with more CH_4 in the mixture, resulting in a dramatic slowdown of the ignition. In the second sub-regime, new H radical, produced through $CH_4 \leftrightarrow CH_3 + H$, became effective, which leveled off the rapid increase in ignition time. As X_{CH4} was further increased, the increased H radical induced a fast procession of $H + CH_4 \leftrightarrow CH_3 + H_2$, which suppressed the main chain-branching reaction $H + O_2 \leftrightarrow OH + O$, leading to a second rapid increase in ignition time.

3.3. Ignition temperature of hydrogen/methane by counter-flowing hot air jets

Non-premixed ignition in counter-flowing fuel, such as H_2 [46–51], methane [52], and higher hydrocarbons [53], vs. hot air

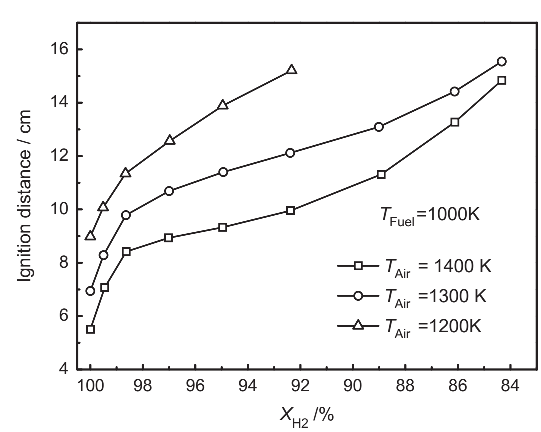


Fig. 7. Ignition distance as a function of X_{H2} for X_{H2} > 85%. Adapted from Ju and Niioka [45]. Three sub-regimes were identified: (a) chain-branching inhibition regime, (b) transition regime, and (c) reaction competition regime.

jets, has been extensively investigated. However, there has been only one paper on the subject of ignition characteristics of hydrogen/hydrocarbon fuel mixtures: Fotache et al. [54] measured the ignition temperature of counter-flowing H_2/N_2 vs. hot air at 1 atm, and the strain rate was fixed at 150 /s. N_2 was then substituted with CH_4 and the corresponding ignition temperature was also measured. Numerically, the ignition temperature of H_2/N_2 was calculated using the mechanism of Kim et al. [55]. The GRI Mech 1.2 [56] was adopted for the H_2/CH_4 system. As shown in Fig. 8, the measured and the calculated ignition temperature for both H_2/N_2 (the squares and the dotted lines) and H_2/CH_4 system (the circles and the solid lines) agree well, except for $X_{H2} > 30\%$ in the H_2/CH_4 system; the GRI Mech1.2 results deviated substantially with the measurements. A modified mechanism based on GRI Mech1.2 was developed (dashed lines). Three distinct regimes were observed. When X_{H2} is less than 6–7%, the H_2/N_2 system failed to ignite and the ignition temperature of H_2/CH_4 was significantly decreased, even with small hydrogen concentrations. For X_{H2} between 7% and 30%, the ignition temperature of methane still decreased, but much less significantly than in the first regime. When X_{H2} was larger than 30%, the ignition temperature was almost independent of the hydrogen concentration.

In Section 3.2, the work of Ju and Niioka [45] is reviewed; it also identified three ignition regimes, but at high hydrogen concentrations. Ju and Niioka's results show the strong inhibitive effect of methane at high hydrogen concentrations. This is in contrast to the results of Fotache et al. [54], in which as much as 70% methane concentration changes ignition temperature very little. This qualitatively different behavior was explained by Fotache et al. as follows: first, the characteristic residence time in Ref. [45] is considerably shorter than in Ref. [54]. Fotache et al. found that at high strain rates (10^4–$10^5\ s^{-1}$), the ignition temperature becomes sensitive to methane addition – even for a small amount of methane [54]. Second, the mechanism Ju and Niioka used imposed a higher rate of H scavenging reaction, which renders a higher sensitivity of methane addition. Finally, the short residence time in Ref. [45] requires the heating of the fuel jet to 1000 K; thus the reaction zone is closer to the fuel side than in Ref. [54], and the effect of methane is further enhanced.

4. Shock tube ignition delay times of hydrogen/hydrocarbons

It is widely recognized that knock in ICEs is caused by the auto-ignition of the end gases. Additionally, developing a controlling strategy in HCCI engines (homogeneous charge compression ignition) requires an understanding of the auto-ignition characteristics of the combustible mixture [57]. Auto-ignition is the chemical reaction of a combustion mixture, which releases energy at a rate sufficient to sustain combustion without an external energy source, such as a spark. Typical auto-ignition involves physical processes (such as heat conduction, diffusion and mixing of reactants) and chemical processes which have characteristic times that combine to form an ignition delay time [58]. Ideally, ignition delay time is defined as the characteristic chemical time for ignition; thus experiments are designed to minimize the time associated with the physical process. One way is to use the homogeneous mixture in which diffusion of heat and mass is absent. In this way, the auto-ignition process is governed by chemical kinetics of pre-flame reactions. During this period of time, there is a rapid depletion of the primary fuel, high radical concentration and an exponential rise in pressure and temperature; all these processes are governed by chemical kinetics. Thus ignition delay time is not only important in understanding the knock phenomenon in ICEs and developing HCCI controlling strategy, but it has been frequently used to validate chemical kinetic mechanisms.

Ignition delay times of hydrocarbons or hydrogen have been measured using a variety of devices, such as the flow reactor [59,60], rapid compression machine [61,62], and the shock tube method [63–75]. The shock tube technique is the most widely used experimental technique for ignition delay time measurement because it can generate a high temperature environment under well-controlled test conditions.

4.1. Non-ideal shock conditions

Ideal shock condition assumptions (constant internal energy, U, and volume, V) used to determine the state of the gas in the reflected shock region do not always hold because of the growth of the boundary layer along the shock tube. Fig. 9(a) shows the typical ignition delay time definition using the reflected shock

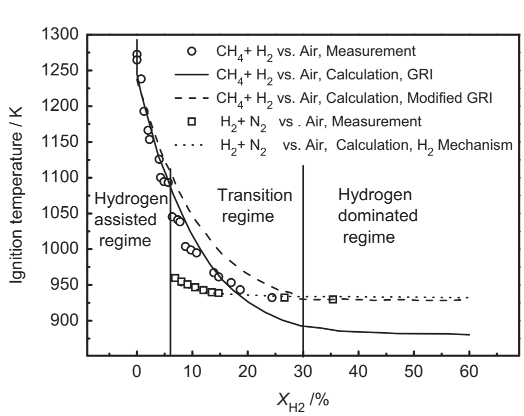


Fig. 8. Ignition temperature as a function of X_{H2}. Adapted from Fotache et al. [54]. Conditions: 1 atm, strain rate $\kappa = 150\ s^{-1}$.

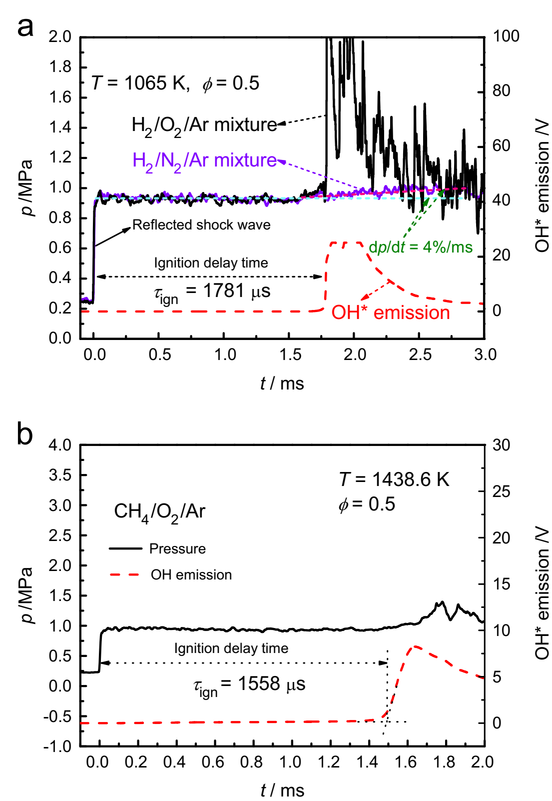


Fig. 9. Typical pressure profile (black solid line) and OH⁎ emission signal (red dash line) show ignition delay in lean hydrogen/oxygen/argon mixture at $T = 1065$ K and $p = 0.95$ MPa. Constant pressure sustained at about 1700 μs [65]. (For interpretation of the references to color in this figure caption, the reader is referred to the web version of this paper.)

wave method. The ignition delay time is defined as the interval between the arrival of the reflected shock wave and the onset of ignition. The onset of ignition can be identified by the steep increase in pressure, as well as the OH* emission. It is seen that even for non-reactive argon-diluted hydrogen/nitrogen, there is still a 4%/ms rise in the pressure rate. This pressure increase exists inherently due to the shock tube boundary layer effect and thus increases the temperature. For weak ignition, where there is no steep increase in pressure (Fig. 9(b)), the ignition delay time should be defined based on the OH* emissions [65–68,74].

Fig. 10 shows the ignition delay times of stoichiometric hydrogen in argon-diluted oxygen reported in the literature. Measurements of Zhang et al. [65], Pang et al. [68], and Herzler and Naumann [76] were plotted as representative data, in comparison with numerical predictions, by using several kinetic mechanisms, including GRI 3.0, Li et al.'s mechanism [77], USC Mech, and Konnov et al.'s mechanism [78]. It is seen that at temperatures higher than around 1050 K, predictions from different kinetic mechanisms agreed well with each other and also with experimental measurements. However, as the temperature was decreased, GRI 3.0 and Li's mechanism over-predicted the ignition delay times while the USC Mech showed a lower prediction than the measurements. The difference in predicting the ignition delay times among different kinetic mechanisms indicates that the rate for lower temperature reactions requires further investigation. When the temperature was further decreased to around 960 K, predictions from all the three kinetic mechanisms were higher than the measurements, and the difference even exceeded an order of magnitude. The deviation between the predictions of the kinetic mechanism and the experimental measurements has been explored. Petersen et al. [73] provided ignition delay time of syngas air mixtures and the same behavior was observed. They attempted to attribute the discrepancy to the uncertainty in rate of certain reactions, such as $CO+HO_2=CO_2+OH$ in the temperature range. However, reasonable rate adjustments do not resolve the disagreements. Dryer and Chaos [66] argued that the hydrogen–oxygen chemical induction process is significantly perturbed by non-homogeneous effects, which are hard to remove in research experiments in the regime of interest (low temperature and high pressure).

Recently, Pang et al. [68] measured lower temperature ignition delay times of hydrogen in argon-diluted oxygen. The effects of shock tube facility-dependent gas dynamics and pre-ignition energy release were believed to cause the deviation between measurements and kinetic mechanism predictions. When non-ideal shock conditions (modified *U*, *V* assumptions), which include the measured pressure history, were used to determine the state

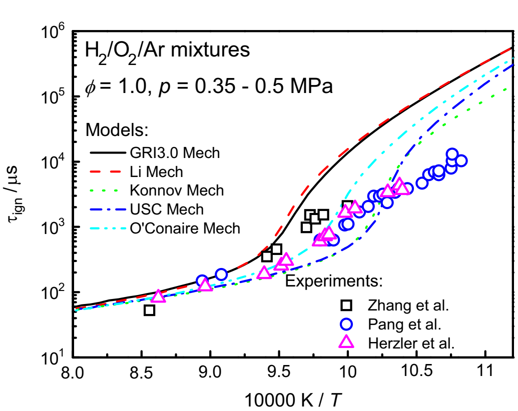


Fig. 10. Comparison of calculated ignition delays using current kinetic models with ideal *U* and *V* assumption to that of the experimental data. All ignition delays normalized to conditions of 0.4 MPa.

of the gas behind the reflected shock wave, the deviations between the model predicted and experimentally measured ignition delay times were finally resolved [68].

There have been extensive investigations on shock tube measurements of ignition delay times of hydrocarbons or hydrogen [63–75]. However, significantly less work has been conducted for hydrogen enriched hydrocarbons. Lifshizt et al. [79] were among the first to experimentally measure the high temperature ignition delay times of methane/hydrogen mixtures using a shock tube. Subsequently, Cheng and Oppenhiem [80] investigated ignition characteristics of methane/hydrogen mixtures and proposed an empirical correlation with the ignition delay time of hydrogen and methane, $\tau=\tau_{CH_4}^{(1-X_{H2})}\tau_{H_2}^{X_{H2}}$. This heuristic formula can qualitatively predict the changes in activation energy at high temperature regions. Gersen et al. [57] measured the ignition delays of stoichiometric methane/hydrogen mixtures with varying hydrogen fractions from 0 to 100% at 1.5–7.0 MPa in a rapid compression machine. The results showed that the promoted effect of the hydrogen addition on methane ignition was only marginal when the hydrogen fraction was less than 20%, while the ignition delays decreased considerably when the hydrogen fraction was over than 50%. Furthermore, Gersen et al. [57] proposed a mixing relation based on the mixing expression (1), suggested by Cheng and Oppenhiem [80], and it can approximate the their experimental data very well. Recently, the Petersen group [72,81] experimentally measured the ignition delays of lean methane/hydrogen mixtures with ratios of 80/20 and 60/40 by using reflected shock waves. The significantly reduced ignition delays were also observed when hydrogen was added. Furthermore, they found that the addition of hydrogen did not seem to shift the dominant kinetic in their study.

Huang et al. [82] conducted both experimental and numerical studies on auto-ignition and chemical kinetics of stoichiometric methane/hydrogen/air mixtures with varying hydrogen fractions from 15% to 35% at high pressure (1.6 MPa and 4.0 MPa) in a shock tube. They reported that the effect of the hydrogen addition on ignition methane was presented and the reduced extent of ignition delays decreased with the decrease in temperature. Chaumeix et al. [83] investigated the shock tube ignition delay and detonation characteristic of methane/hydrogen mixtures; they concluded that the presence of methane significantly inhibits the detonation of the combustible mixtures due to lowered ignition temperature and longer ignition delay of methane.

Herzler and Naumann [76] conducted the experimental and numerical study on ignition delays of methane/ethane/hydrogen mixtures with varying hydrogen fractions from 0 to 100% in a shock tube. Their results showed that the current mechanisms could not well represent the reduction of global activation energy at relative low temperature for high fractions of hydrogen in the fuel mixtures.

More recently, a more systematic investigation on auto-ignition characteristics of methane/hydrogen mixtures was conducted by Zhang et al. [65], and three auto-ignition regimes were identified, depending on the hydrogen fraction: the methane chemistry dominated ignition (MCDI), when the hydrogen fraction was less than 40%; the combined chemistry of methane and hydrogen dominated ignition (CCMHDI), when the mole fraction of hydrogen was about 60%; and the hydrogen chemistry dominated ignition (HCDI), when the hydrogen fraction was more than 80%. Detailed discussion of auto-ignition characteristics, and the corresponding reaction kinetics in each regime, based on the work by Zhang et al. follows.

4.2. Reaction system in MCDI regime

Zhang et al. [65] found that for hydrogen fractions X_{H2} with a less than 40% methane/hydrogen mixture, the ignition characteristics of methane/hydrogen resembles that of pure methane and the ignition

process is governed by the kinetics of methane; thus this regime is defined as the methane-chemistry-dominated-ignition (MCDI) regime. In this regime, the ignition delay time dependence on pressure and equivalence ratio is specified in the following.

4.2.1. *Effect of pressure in MCDI regime*

Fig. 11 shows the ignition delay time of methane/hydrogen in Ar diluted oxygen for $X_{H2}=0$, 20%, and 40%, an equivalence ratio of 0.5, and at elevated pressures. For pure methane fuel, as shown in Fig. 11(a), the logarithmic ignition delay time is a linear function of the inverse temperature; thus an Arrhenius-type correlation, through a multi-regression method, was formulated, as shown in Eq. (6), where $R=1.986\times10^{-3}$ kcal/(mole K) is the universal gas constant, *A*, *B*, *C*, and *D* are correlation parameters and E_a is the global activation energy in kcal/mole. As the pressure increases from 0.5 MPa to 2 MPa, the global activation energy is decreased from 48.4 to 42.8 kcal/mole

$$\tau_{ign}=Ap^{-B}\phi^{C}X_{O2}^{-D}\exp(E_a/RT) \quad (6)$$

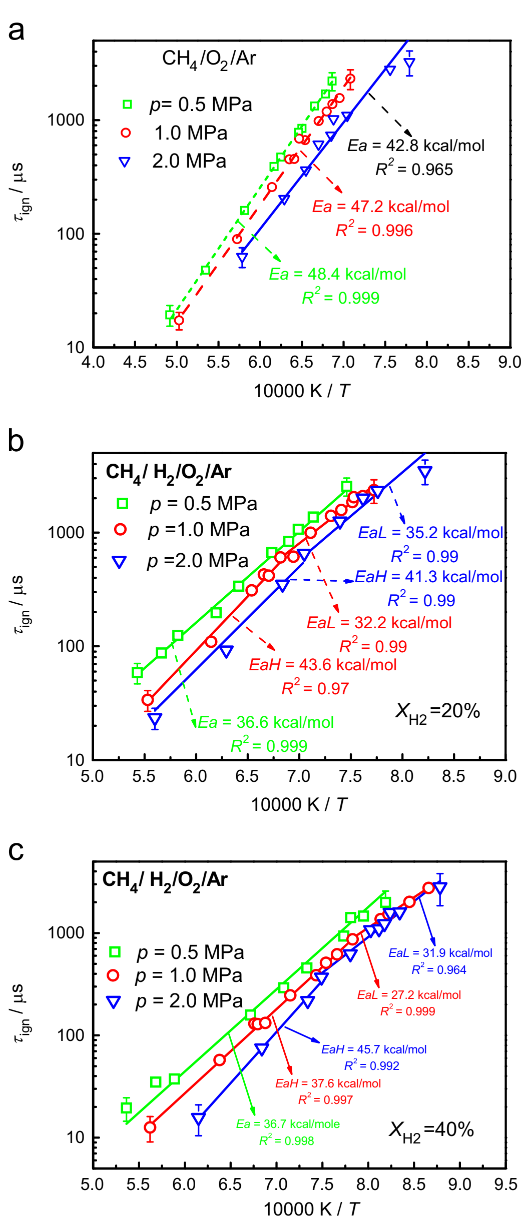


Fig. 11. Effect of pressure on ignition for $XH_2\leq40\%$ in lean methane/hydrogen mixtures with dilution Ar. Adapted from Ref. [65].

Generally, the pressure exponent, *B*, in Eq. (6), is a negative value of around 0.5 for typical hydrocarbon fuels, which implies that ignition delay time is reduced with increasing pressure. Additionally, typical values of the global activation energy of pure methane at the temperature range between 1315 and 2000 K are within the range of 46–54 kcal/mol [72,75,79,80,84,85], as shown in Table 2. Relatively small activation energy (18 kcal/mol) was reported in the study of Huang et al. [86]. It is noted that the dominant chain-branching reactions are quite different in different temperature ranges. The chain-branching reactions $CH_3+O_2\leftrightarrow O+CH_3O$ and $HO_2+CH_3\leftrightarrow OH+CH_3O$ are more important when the temperature is higher than 1400 K. However, the reactions $CH_3+CH_3O_2\leftrightarrow CH_3O+CH_3O$ and H_2O_2 $(+M)\leftrightarrow OH+OH$ $(+M)$ dominate the ignition chemistry when the temperature is lower than 1100 K [69]. Thus the significant difference in global activation energy reported by Huang et al. is caused by the temperature range (1000–1350 K), which they studied. Furthermore, Huang et al. [86] found a reversed "S" shaped characteristic in the methane/air mixture. Petersen et al. [71] suggested that the elevated temperature would not shift the kinetic regimes for the lean methane–oxygen mixtures. Note that the effect of elevated pressure on the ignition kinetic was weakened with an increase in the hydrogen mole fraction in the fuel mixture for MCDI at the relative low temperature region. When the hydrogen was added into methane, as shown in Fig. 11(b) and (c), there was a slight change in the global activation energy for the pressure of 1 and 2 MPa. This is because the hydrogen addition weakened the dominance of the methane chemistry. The similar transition in global activation energy was also observed by Petersen et al. [72], for $X_{H2}=20\%$ CH_4/H_2 fuel blend at a pressure of 2.1 MPa. A high temperature activation energy (E_{aH}) of 41.4 kcal/mol and a low temperature activation energy (E_{aL}), of 31.1 kcal/mol were reported in their study. The transition was attributed to the effect of the hydrogen addition on the chain-branching during the ignition process.

Herzler and Naumann [76] measured the ignition delay times of stoichiometric hydrogen/reference gas (mixtures of 92%

Table 2
Global activation energy of typical hydrocarbon fuels.

Source	Experimental conditions	Activation energy (kcal/mol)
Zhang et al. [65]	$T_5=1290$–2000 K $p_5=0.5$–2.0 MPa $\phi=0.5$ Ar = 80%	42.8–48.4
Grillo and Slack [84]	$T_5=1400$–1850 K $p_5=0.4$ MPa $\phi=2.0$ Ar = 79–96%	53.4
Seery and Bowman [85]	$T_5=1350$–1900 K $p_5=0.15$–0.4 MPa $\phi=0.2$–5.0 Ar = 53.4–78.4%	52.3
Petersen et al. [72,75]	$T_5=1410$–2040 K $p_5=0.9$–48 MPa $\phi=0.5$–4.0 Ar = 89–99%, $N_2=97.66\%$	51.8
Lifshitz et al. [79]	$T_5=1500$–2100 K $p_5=0.2$–1.0 MPa $\phi=0.5$–2.0 Ar = 89–97%	51.4
Cheng and Oppenheim [80]	$T_5=800$–2400 K $p_5=0.1$–0.3 MPa $\phi=0.5$–1.5 Ar = 90%	46.4

methane and 8% ethane) in Argon-diluted oxygen (dilution ratio 1:5), and their measurements, along with numerical predictions, using USC Mech II at the exact conditions presented in Fig. 12. Excellent agreement between the measurements and the numerical predictions was observed in the temperature range studied in Ref. [76]. The ignition delay time of the reference gas (shown in Fig. 12(a)) decreased with increasing pressure with a factor of $p^{0.5}$, which is typical for hydrocarbons. Their data for the equivalence ratio of 0.5 were not plotted here, and all the data for the reference gas can be fitted by

$$\tau_{ign}/\mu s = 10^{-2.75 \pm 0.13}(\mathrm{p/bar})^{-0.51 \pm 0.02}\phi^{0.59 \pm 0.06} \times \exp(20,450 \pm 442\ \mathrm{K}/T) \quad (7)$$

yielding a global activation energy of 40.46 kcal/mole.

4.2.2. Effects of equivalence ratio in MCDI regime

Fig. 13 shows the ignition delay time of methane/hydrogen in Ar diluted oxygen for the equivalence ratio of 0.5, 1.0 and 2.0 at the pressure of 2 MPa. It is seen that two temperature regions were classified, based on the changes in global activation energy. At the high temperature region, ignition delay times increased with the increasing equivalence ratio, indicating that the lean mixture had higher reactivity during the ignition process. The ignition kinetic depends more on oxygen concentrations at high temperature regions because the chain-branching reaction $H+O_2=OH+O$ is facilitated for leaner mixtures (higher oxygen concentration), in the high temperature range, and thus promotes the ignition of the mixtures and reduces the ignition delay times.

When the temperature is decreased (demonstrated by the open symbols in Fig. 13), a similar dependence on equivalence ratio is presented: the ignition delays of mixtures increased with the increasing equivalence ratio. However, the overall slope of the logarithmic ignition delay time – or the global activation energy – was significantly lower than at high temperatures. When the temperature was decreased, the fuel-specific reactions became more important in governing the ignition. Specifically, the concentration of methane increased with the increased equivalence ratio, leading to the increased production of methyl radicals, which in turn promoted the chain termination reaction $CH_3+CH_3\ (+M) \leftrightarrow C_2H_6\ (+M)$, and increased the ignition delay time. Additionally, the chain-branching reaction $H+O_2 \leftrightarrow OH+O$ at high temperatures has a higher activation energy than the methyl radical production reactions by H abstraction from methane, resulting in the observed, more gentle slope at lower temperatures.

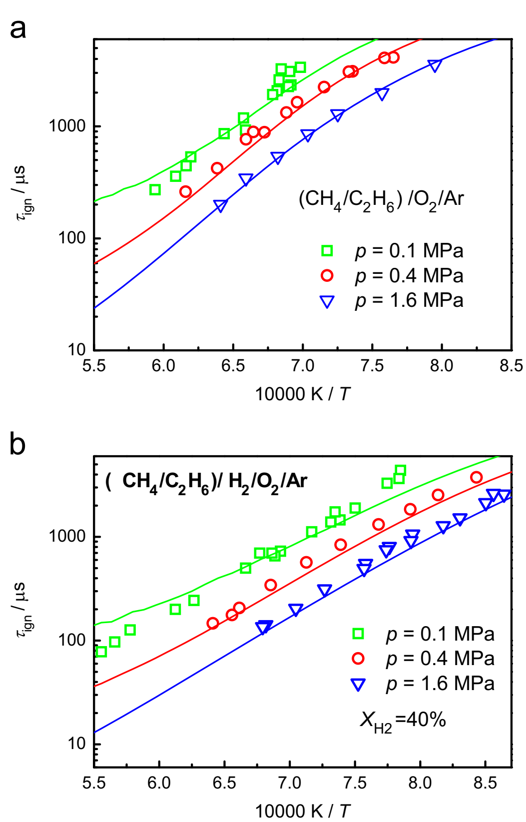


Fig. 12. Effect of pressure on ignition for $XH_2 \leq 40\%$ in stoichiometric methane/ethane/hydrogen mixtures with dilution Ar. Experiments: symbols: obtained from Herzler et al. [76]. Simulations: lines: USC 2.0 Mech [134] with dp/dt=4%/ms.

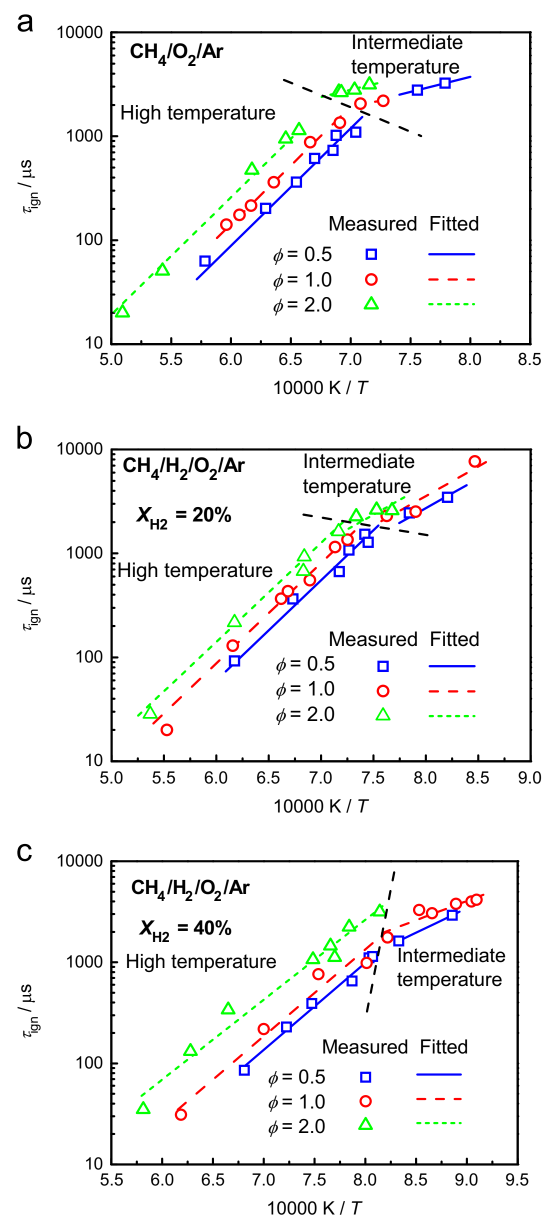


Fig. 13. Effect of equivalence ratio on ignition for MCDI mixtures with dilution Ar. Adapted from Ref. [65].

4.3. Reaction system in CCMHDI regime

4.3.1. Effects of pressure in CCMHDI regime

For X_{H2} around 60%, Zhang et al. proposed that the ignition delay time of the methane/hydrogen in Ar diluted oxygen is governed by the combined chemistry of methane and hydrogen

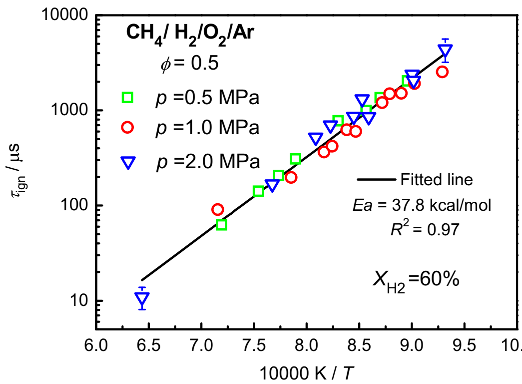


Fig. 14. Effect of pressure on ignition delay for CCMHDI mixture. Adapted from Ref. [65].

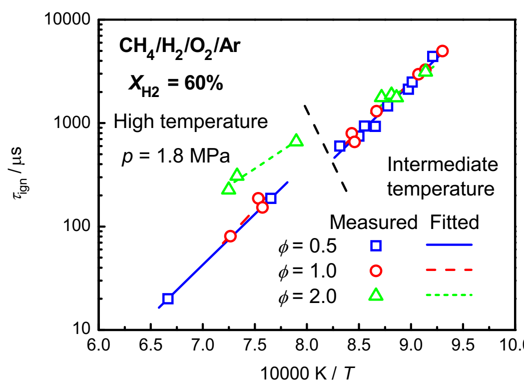


Fig. 15. Effect of equivalence ratio on ignition delay for CCMHDI mixture. Adapted from Ref. [65].

dominated ignition (CCMHDI). Fig. 14 shows the ignition delay time of methane/hydrogen mixtures for the equivalence ratio of 0.5 and a pressure of 0.5, 1 and 2 MPa. Unlike the pressure behavior in the MCDI shown in Fig. 11, the ignition delay times at the three pressures investigated approach the same value, which implies that the pressure imposes only subtle influence on the ignition delay time. The pressure dependence is different from those of MCDI mixtures. An Arrhenius-type expression with $R^2=0.97$ is correlated using the multiple linear regression method based on the normalized pressure of 1.0 MPa

$$\tau_{ign}/\mu s = 10^{-4.1 \pm 0.23}(p/\text{bar})^{-0.00629}\exp(19,100 \pm 623\ K/T) \qquad (8)$$

The insensitivity of the ignition delay time on pressure for CCMHDI mixtures was reasonable because for methane the pressure imposed a promoting effect on ignition, as seen in Eq. (7). However, when the pressure was increased for argon-diluted hydrogen/oxygen mixtures, the termination reaction $H+O_2=HO_2$ is favored. Thus the net effect was the observed weak dependence of the ignition delay time on pressure.

4.3.2. Effects of equivalence ratio in CCMHDI regime

For the CCMHDI mixture, Fig. 15 shows ignition delay time for the equivalence ratio of 0.5, 1.0 and 2.0. In the high temperature region, the ignition delay time for $\phi=1.0$ is slightly higher than $\phi=0.5$, while the ignition delay for $\phi=2.0$ is significantly higher. This non-linear variation of the logarithmic ignition delay time with the equivalence ratio indicates that similar correlation as Eq. (7) for the ignition delay time as a function of the equivalence ratio is not available.

In the middle-low temperature region, ignition delay times are insensitive to the change of equivalence ratio. A similar phenomenon was reported by Gersen et al. [57]; the reason is that ignition is now governed by the combined chemistry of methane and hydrogen. The typical reactions that favor ignition are the chain-branching reaction $H+O_2 \leftrightarrow OH+O$, while the most effective ignition inhibiting reaction is H radical consumption reaction $CH_4+H \leftrightarrow CH_3+H_2$. As the equivalence ratio is increased, the hydrogen concentration increases, leading to increased production of H radicals and consequently, decreased ignition delay time. On the other hand, the concentration of methane also increases, which consumes the H radical and increases the ignition delay time. Thus the insensitivity of delayed ignition time on the equivalence ratio in the temperature range is caused by the combined chemistry of methane and hydrogen.

4.4. Reaction system in HCDI regime

For X_{H2} higher than 80%, it is believed that the ignition behavior of methane/hydrogen fuel mixtures is dominated by hydrogen chemistry, and Zhang et al. [65] proposed that ignition behavior of this type of fuel mixtures to be hydrogen chemistry dominated ignition (HCDI).

4.4.1. Effect of pressure in HCDI regime

Fig. 16 shows the ignition delay time for $X_{H2}=80\%$ methane/hydrogen fuel mixtures in argon-diluted oxygen at the equivalence ratio of 0.5, and elevated pressures. It is seen that when ignition delay time versus inverse temperature, there is a significant transition in slope, indicating a change in the overall activation energy. Skinner and Ringrose [87] investigated the ignition delay time of pure hydrogen in oxygen (argon-diluted); their results also showed two transitions in overall activation energy with increased temperature. At higher temperatures ($T > 1200$ K), the ignition delay time exhibited a negative dependence on pressure, indicating that the overall reactivity increased with the increasing pressure. An opposite pressure dependence is presented at intermediate temperature. This observation is consistent with the study of Herzler and Naumann [76] for methane/ethane/hydrogen mixtures. The reason is that when hydrogen fraction is over 80%, ignition is governed primarily by hydrogen chemistry. The competition between reactions $H+O_2\,(+M) \leftrightarrow HO_2\,(+M)$ and $H+O_2 \leftrightarrow OH+O$ is believed to result in complex pressure dependence. Specifically, the ignition delay time of the HCDI system at 2.0 MPa and for $T < 1200$ K is higher than at 0.5 and 1.0 MPa because reaction $H+O_2\,(+M) \leftrightarrow HO_2\,(+M)$ is facilitated at higher pressures. While for higher temperatures and typical hydrocarbon chemistry dominated ignition, the higher absolute concentrations due to higher pressures will promote the chain-branching reaction $H+O_2 \leftrightarrow OH+O$, thus decreases ignition delay time, as observed in Fig. 16 for temperatures higher than 1100 K and in Figs. 11–14 for typical hydrocarbon chemistry dominated ignition.

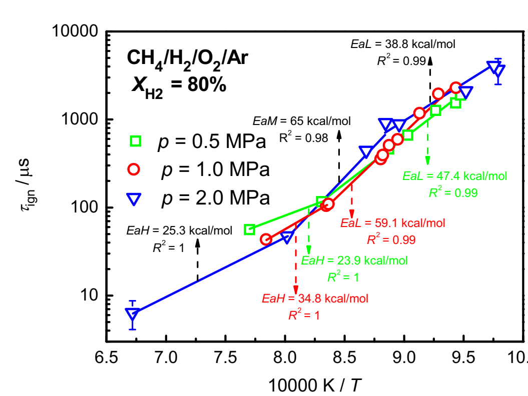


Fig. 16. Effect of pressure on ignition delay for HCDI mixtures (20% methane/80% hydrogen). Adapted from Ref. [65].

In addition, Fig. 16 shows that the crossing of data at 1.0 and 0.5 MPa shifted to even lower temperatures (1100 K). This observation can, by the same token, be explained by the fact that reaction $H+O_2$ (+M) $\leftrightarrow HO_2$ (+M) – if preferably facilitated over the reaction $H+O_2 \leftrightarrow OH+O$ at relatively higher pressure and lower temperature.

4.4.2. *Effect of equivalence ratio in HCDI regime*

Fig. 17 shows the ignition delay time for 80% reference gas/20% hydrogen fuel mixtures in argon-diluted oxygen at 0.1 MPa and the equivalence ratio of 0.5 and 1.0 [76]. The ignition delay time increases with the increase of equivalence ratio because, in this temperature range, reducing the oxygen concentration retards the chain-branching reaction $H+O_2 \leftrightarrow OH+O$ and consequently inhibits ignition.

However, Herzler and Naumann [76] showed that at higher pressure (1.6 MPa) a weak influence of equivalence ratio occurred in the ignition delay time for the HCDI mixture, as shown in Fig. 18(a). In the lower temperature region ($T<1160$ K), ignition delay times at the equivalence ratio of 0.5 and 1.0 were almost identical. When the temperature was increased to 1250 K, the ignition delay time at $\phi=0.5$ was slightly lower than at $\phi=1.0$. This observation is consistent with the results of Zhang et al. [65], who measured ignition delay times for $X_{H2}=80\%$ hydrogen/methane in argon-diluted oxygen at 1.8 MPa for $\phi=0.5$, 1.0, and 2.0, as shown in Fig. 18(b). It is seen that in lower temperature regions, the ignition delay time for three equivalence ratios was almost the same, while at higher temperatures, the ignition delay time increased with the increased equivalence ratio.

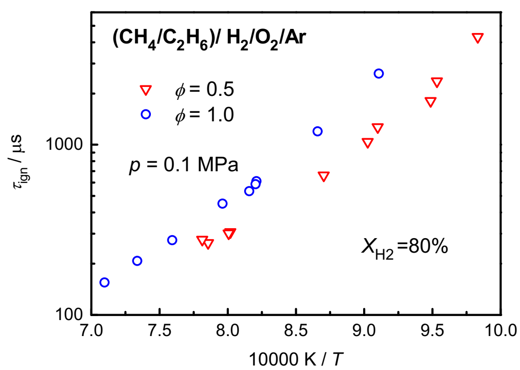


Fig. 17. Effect of equivalence ratio on ignition delay for HCDI mixture at low pressure. Experiments: symbols: obtained from Herzler et al. [76]. Simulations: lines: USC 2.0 Mech [134] with dp/dt=4%/ms.

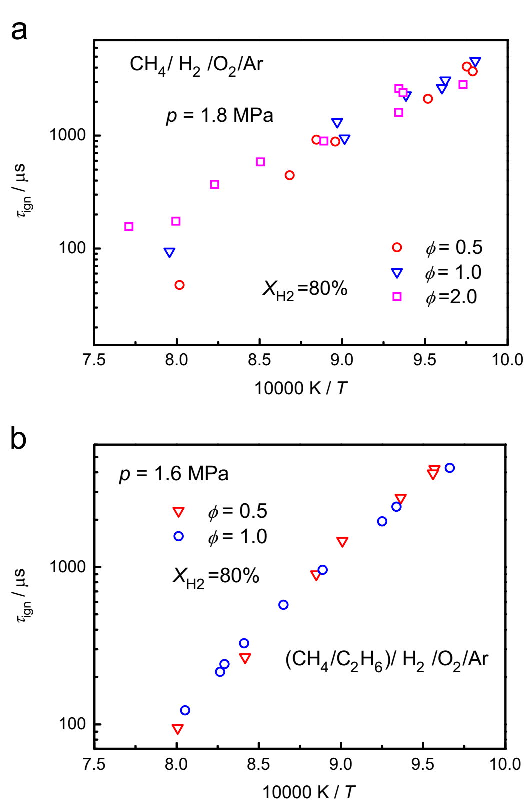


Fig. 18. Effect of equivalence ratio on ignition delay for HCDI mixtures. Adapted from Ref. [65].

5. Laminar flame speed and flame front instability

5.1. *Laminar flame speed*

Laminar flame speed is a physiochemical property of a combustible mixture, which characterizes its diffusivity, reactivity and exothermicity [25]. Accurately measured laminar flame speed can be used to validate chemical kinetic mechanisms [88–90] in engine design [91] and in turbulent combustion modeling [92–94].

Hydrocarbon oxidation mechanisms have been reported and reviewed extensively [89,90]; and they have been greatly improved, enabling the numerical prediction of laminar flame speed of each single-fuel/oxidizer system. However, there is still no method for calculating the laminar flame speed of hydrogen/hydrocarbon/air mixtures, because the oxidation mechanisms of fuel blends cannot be the simple combinations of the mechanisms of all the constituent fuels. Thus experiments are required to obtain the laminar flame speed data for hydrogen/hydrocarbon fuel blends.

Methods for measuring laminar flame speed include the stagnation plane flame method [95], the heat flux method [96,97], and the combustion bomb method [98–103]. The stagnation plane flame method utilizes the stable flow of premixed combustible mixtures and the flow velocity was profiled through which the strain rate is extracted. When the flow velocity was extrapolated to zero strain rate, the laminar flame speed was determined. The heat flux method extrapolates the heat flux to zero to obtain the adiabatic flame speed. While these two methods are easy, because the parameters to be measured are stable quantities. However, typically the flame speed at high pressures is difficult to be measured through the stagnation plane flame method or the heat flux method because at high pressures, stable combustion is inherently difficult to achieve. The combustion bomb method introduces outwardly propagating spherical flame and has been widely used because of its simple flame configuration, well-defined flame stretch rate and well-controlled experimentation [98,99], making it the most widely used experimental technique for flame speed measurements. The first outwardly propagating spherical flame was imaged and reported by Manton et al. [104]; however, their focus was on flame morphology, e.g., flame cellularity caused by preferential diffusion. The first flame speed measurements with schlieren observation were reported in 1969 by Palm-Leis and Roger [105]; they attributed the changes in flame speed in spherical explosions to flame stretch. In addition, most previous experimental reports on laminar flame speeds measurements used hydrogen/air [99,106–110], or hydrocarbons/air [96–98,111–125], mixtures and there is relatively less literature on the effects of hydrogen addition on the laminar flame speed of hydrocarbon/air mixtures [95,100–103,126–128]. Although the definitions of hydrogen addition extent used in these studies were different, qualitatively, all these studies show that laminar flame speed increases when more hydrogen is added. The definition of

each hydrogen addition parameter and presentations of the flame speed variation of each parameter follows.

5.1.1. Laminar flame speed versus X_{H2}

Currently, most researchers use X_{H2} to quantify the hydrogen addition extent because is the simplest quantification parameter [100–102,127,129–132], possessing significant merit in engineering applications, such as in hydrogen/natural gas spark ignition engines [133].

5.1.1.1. H_2/natural gas or methane. Huang et al. [100] studied the effects of hydrogen addition on laminar flame speeds of natural gas at 1 atm and room temperature; they found that normalized flame speed increased quasi-exponentially with X_{H2}. An empirical correlation between the laminar flame speed and X_{H2} was deduced from the experimental observations, as shown in the following equation:

$$\frac{S_u^0(\phi, X_{H2}) - S_u^0(\phi, 0)}{S_u^0(\phi, 1) - S_u^0(\phi, 0)} = 0.00737 \exp\left(\frac{X_{H2}}{0.2038}\right) + 0.00334 \quad (9)$$

Methane is a major component of natural gas and the laminar flame speed of hydrogen/methane/air mixtures has been computationally [126], and experimentally [127] studied. Three distinct regimes of flame speed behavior, with increasing X_{H2} was identified, as shown in Fig. 19. When $0 < X_{H2} < 0.6$ (Regime I), the laminar flame speed increased slightly with increasing X_{H2}, indicating that in this regime, the combustion was dominated by methane. When X_{H2} is higher than 0.8 (Regime III), the laminar flame speed decreased dramatically with decreasing X_{H2}, indicating that the presence of small amount of methane can greatly inhibit hydrogen/air flame propagation. When $0.6 \leq X_{H2} \leq 0.9$ (Regime II), the flame speed increased by increasing X_{H2} is respectively more and less significant than Regimes I and III.

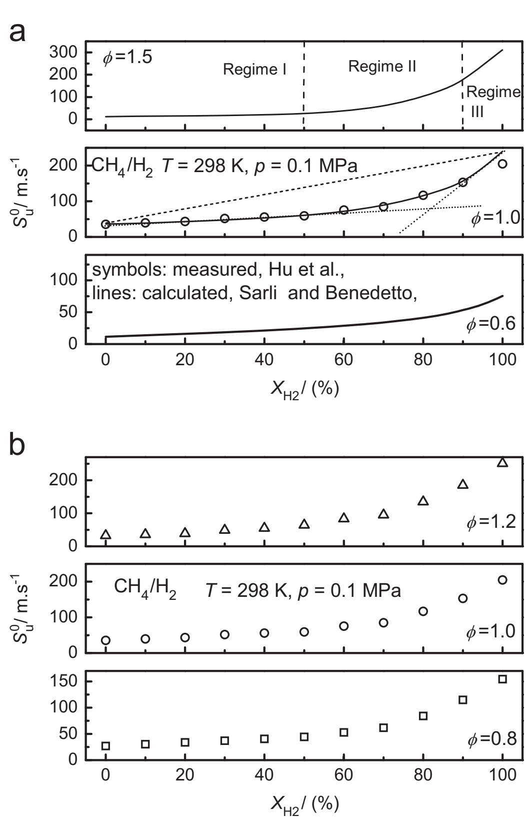


Fig. 19. Laminar flame speed of hydrogen/methane/air mixtures as a function of X_{H2} at $\phi = 1.0$. Scatters: measurements (data source: Ref. [127]), lines: calculations (*data source*: Ref. [126]).

5.1.1.2. H_2/propane. The laminar flame speed of stoichiometric hydrogen/propane/air mixtures was experimentally reported by Milton and Keck [91], using the closed bomb method. Their results were obtained through thermodynamic calculation based on the pressure history; their calculated flame speed has complex dependence on the initial temperature and pressure, as shown in Fig. 20. When the H/C ratio is 8 (equivalent to $X_{H2} = 0.89$), laminar flame speed is much higher than when H/C ratio equals 4 (equivalent to $X_{H2} = 0.67$).

Recently, Law and Kwon [128] studied the hydrocarbon substitution effect on atmospheric hydrogen air propagation with an outwardly spherical flame. They measured the flame speed of atmospheric hydrogen/air with small amounts of hydrocarbon substitution; the laminar flame speeds were plotted against the specifically defined SFHC (stoichiometric fraction of hydrocarbon, defined as $5X_{C3H8}/(0.5X_{H2} + 5X_{C3H8})$, Ref. [128]). Tang et al. also measured the flame speed of propane with an increasing hydrogen addition extent at atmospheric pressure, room temperature [102], and elevated pressures and temperatures [101]. The objectives of Law and Kwon and Tang et al. were quite different: Law and Kwon [128] focused on the hydrocarbon addition effect on hydrogen/air flame propagation, while Tang et al. [101] – with a practical and simply-defined hydrogen addition extent – measured the flame speed of propane with a hydrogen addition. The SFHC defined in Ref. [128] were converted to X_{H2} in Ref. [101], and their results of propane/hydrogen flame speeds were plotted in Fig. 21 as a function of X_{H2}. It clearly shows that for X_{H2} larger than 80%, laminar flame speed increased dramatically with the increase of X_{H2}. The results of Law and Kwon covered the high X_{H2} (low SFHC), range and the results of Tang et al. [101], being quite the opposite, covered the whole range, but very sparsely at high X_{H2}. However, it was found that a simple fitting of the results of Tang et al. overlaps the results of Law and Kwon, thus unifying the definitions of X_{H2} and SFHC.

The results of Tang et al. [101] were then compared with the computationally predicted values. The mechanism they used was the recently developed and highly cited USC Mech II [134], for high temperature oxidation of H_2/CO/C1-C4 compounds. It showed that agreement between the experimental and computational results was excellent at low atmospheric pressures, while discrepancies still existed for higher pressures. This shows the irreconcilable difference between experimental measurements and computational predictions.

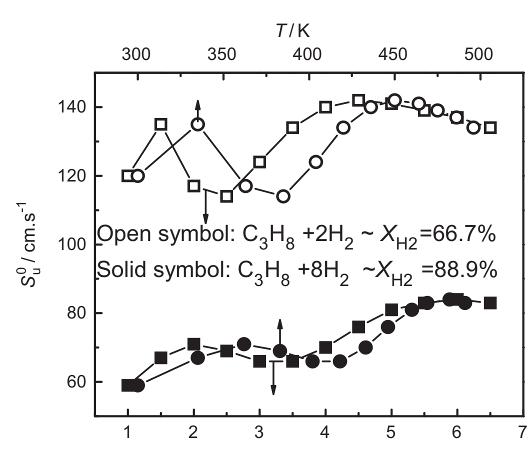


Fig. 20. Laminar flame speed of stoichiometric hydrogen/propane/air mixtures as a function of temperature and pressure. *Data source*: Ref. [91].

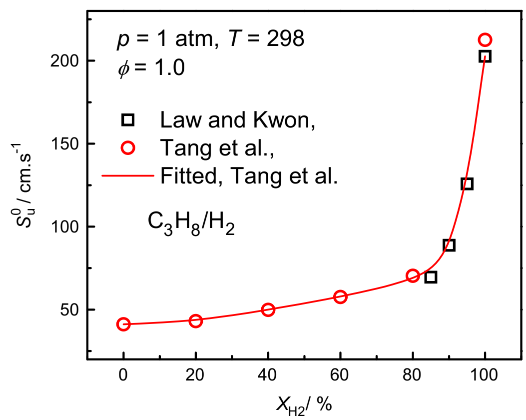


Fig. 21. Flame speed of Law and Kwon [128] and Tang et al. [101] as a function of X_{H2}.

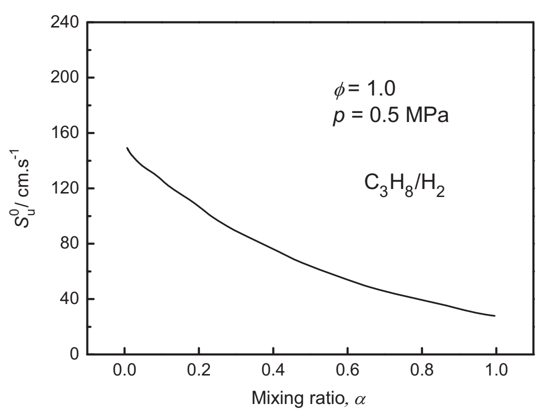


Fig. 22. Experimental (points) and calculated (line) laminar flame speeds as a function of 5 atm and overall equivalence ratio of 1.0, adapted from Law et al. [135].

The results of Law et al. [135] were also presented here, in Fig. 22. The figure clearly shows that both experimentally measured and computationally predicted flame speed decreased with the increase of propane addition. At a lower mixing ratio (higher hydrogen fraction), the agreement between the experiments and the computations becomes bad because the mechanism of Qin et al. [136] was developed for C1–C2 hydrocarbons and could not degenerate to the hydrogen oxidization mechanism as the mixing ratio decreases (hydrogen fraction increases).

The dependence of laminar flame speed on temperature and pressure is discussed in Ref. [101]. Laminar flame speed decreases monotonically with the increase of P_u and increases quasi-linearly with the increase of T_u. As the pressure increases, the intensity of the temperature-sensitive, two-body, branching reaction: $H+O_2 \leftrightarrow OH+O$ is approximately fixed, due to the insensitivity of adiabatic temperature to the increase in pressure, while the three-body, temperature-insensitive, inhibiting reaction: $H+O_2+M \leftrightarrow HO_2+M$ is enhanced, and a retarding effect is therefore imposed on the overall progress of the reaction with increasing pressure. However, this effect is not great enough to be responsible for the trend of the flame speed to decrease with the increasing pressure because the pressure effect of the chain mechanism can be quantified through the overall reaction order n (typically in the range of 1–2), which can be locally defined as $f^0 \sim p^{n/2}$. Thus the flame speed $\sim f^0/\rho_u \sim p^{n/2-1}$ shows that the decrease in flame speed with the increasing pressure is actually caused by increasing pressure [137–139]. The increase in the upstream temperature increases the adiabatic temperature, which influences the reaction rate; the dependence is more sensitive for larger values of T_u because of the Arrhenius factor.

5.1.1.3. H_2/higher hydrocarbons. Mandilas et al. [140] measured the laminar flame speed of hydrogen/*iso*-octane/air mixtures. About 5% by mass of hydrogen was added (equivalent to $X_{H2}=0.75$) into the base fuel and it was observed that the laminar flame speed of hydrogen/iso-octane/air mixtures was higher than those of pure *iso*-octane/air mixtures over the equivalence ratio range between 0.8 and 2.0.

5.1.2. Laminar flame speed versus R_H

5.1.2.1. Definition of R_H. In 1984, Yu et al. [95] used the symmetric counter-flow flame to accurately measure the flame speeds of propane–air with stoichiometrically small amounts of hydrogen addition. In their study, it was assumed that the hydrogen only presents in small amounts and is completely consumed by part of the total air; in consequence the remaining air is the oxidizer defining the mixture stoichiometry. Thus, the stoichiometry was defined through the mole fraction of hydrogen (C_H), propane (C_F), and air (C_A) as

$$\phi_F = \frac{C_F/[C_A - C_H/(C_H/C_A)_{stoic}]}{(C_F/C_A)_{stoic}} \tag{10}$$

where the subscript represents the stoichiometric value (for instance, $(C_H/C_A)_{stoic}$ is the stoichiometric fuel-to-air molar ratio); the remaining air for hydrocarbon oxidation is represented by the term in brackets.

The extent of hydrogen addition was then correspondingly defined as

$$R_H = \frac{C_H + C_H/(C_H/C_A)_{stoic}}{C_F + [C_A - C_H/(C_H/C_A)_{stoic}]} \tag{11}$$

It should be pointed out that the parameters ϕ_F and R_H indicate the mixture concentration and the relative amount of added hydrogen. In addition, it is easy to discover that the two parameters do not represent the actual stoichiometry during the reaction, but they do facilitate data reduction and correlation, which will be discussed in detail in the following.

5.1.2.2. Linearity between the laminar flame speed and R_H. Fig. 23 shows the laminar flame speed of hydrogen enriched methane and propane–air mixtures as a function of R_H at 1 atm and room temperature [95]. The scatters were the experimental results and it is seen that the linear fitting (lines) correlates the laminar flame speed very well with R_H. Yu et al. [95] derived the following correlation for the laminar flame speed of hydrogen enriched methane and propane fuel mixtures:

$$S_u^0(\phi_F, R_H) = S_u^0(\phi_F, 0) + 83R_H \tag{12}$$

Eq. (12) indicates that the laminar flame speed is a linear function of R_H; in addition, the slope of linearity is independent of the effective equivalence ratio, which means that the hydrogen addition effect is quantitatively the same for different effective equivalence ratios. This correlation has elicited substantial follow-up investigations because of the interest of hydrogen combustion and its simplicity.

Sher and Ozdor [141] have determined the laminar flame speed of hydrogen enriched butane/air mixtures by thermodynamic calculations based on the flow rate of the mixture and heat carried away by the cooling water.

Since the mid-1980s, the accuracy of the determination of laminar flame speed has enabled important improvements due to the development of experimental techniques such as high speed

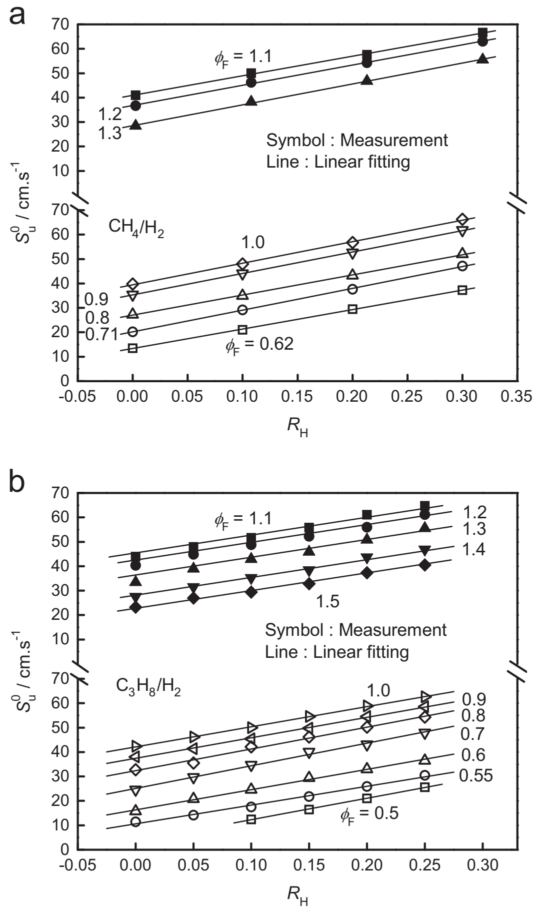


Fig. 23. Laminar flame speed of hydrogen enriched (a) methane and (b) propane as a function of R_H. Data re-plotted from Yu et al. [95].

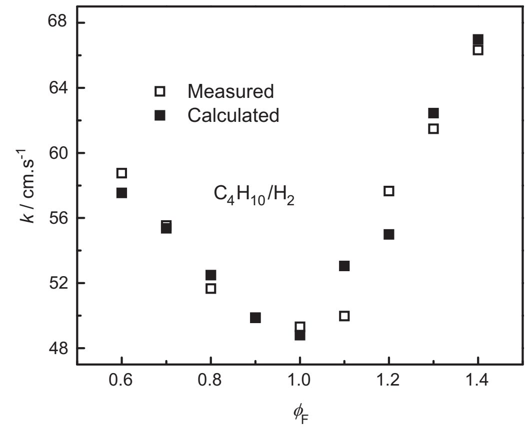


Fig. 24. Linearity coefficient, k, quantifying the increase in flame speed with R_H [103].

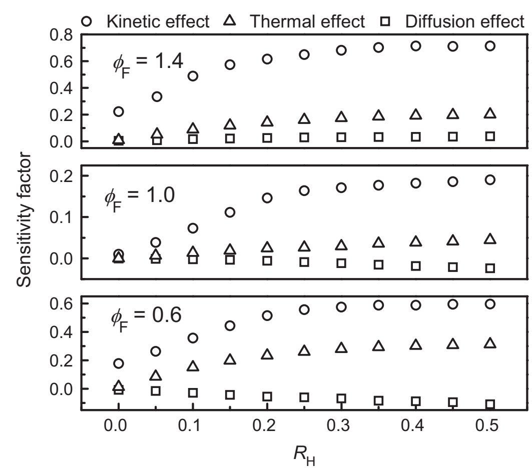


Fig. 25. Sensitivity coefficients measuring kinetic, thermal, and diffusion effects on laminar flame speeds, with hydrogen addition, as functions of R_H [103].

photography, more sophisticated data processing methods such as non-linear extrapolation techniques for removal of stretch effect, and the routinely used computational simulations of 1D freely propagating planar flame. Using the above concepts, Tang et al. [103] experimentally re-examined and extended the linear correlation between the laminar flame speed and R_H to hydrogen/butane/air mixtures. Both measurements and computations show that the linear correlation still holds for hydrogen/butane–air mixtures, the following correlation was proposed:

$$S_u^o(\phi_F, R_H) = S_u^o(\phi_F, 0) + k(\phi_F)R_H \tag{13}$$

As we mentioned previously, Eq. (13) simply correlates the laminar flame speed with the parameters ϕ_F and R_H, while the empirical correlation of Eq. (9) is more complicated. However, the underline factor is consistent: the laminar flame speed of the hydrogen/hydrocarbon mixture depends strongly on the mixture richness and hydrogen addition level.

Unlike the statement of Yu et al. [95] that the slope was a constant for all effective equivalence ratios, Tang et al. [103] discovered that the slope of the linear correlation, k, depends strongly on the effective equivalence ratio, ϕ_F, as shown in Fig. 24. The linear dependence is weakened as the mixture is close to stoichiometry. In other words, the hydrogen addition effect is minimized at around stoichiometric condition.

Fundamentally, when a certain amount of hydrogen is added to hydrocarbon, the laminar flame speed is influenced by three mechanisms: (a) the thermal effect, caused by the higher adiabatic flame temperature of hydrogen; (b) the transport effect caused by the high mobility of hydrogen; (c) the kinetic effect due to the strong reactivity of hydrogen. Because the laminar burning flux (which is the eigenvalue for flame propagation) is given by

$$f^2 \sim Le \exp(-E_a/R^0 T_{ad}) \tag{14}$$

in which the Lewis number Le, the activation energy E_a, and the adiabatic flame temperature T_{ad} can be considered to, respectively, represent the diffusion, kinetic, and thermal effects. To assess the relative importance of the three factors, Eq. (14) was differentiated to give the overall sensitivity coefficient as

$$\frac{\partial \ln f}{\partial \ln R_H} \sim \frac{1}{2Le}\frac{dLe}{d \ln R_H} - \frac{1}{2T_{ad}}\frac{dT_a}{d \ln R_H} + \frac{T_a}{2T_{ad}^2}\frac{dT_{ad}}{d \ln R_H} \tag{15}$$

where $T_a = E_a/R^o$ is the activation temperature and the three terms on the right respectively represent the individual sensitivity coefficients for diffusion, kinetic, and thermal effects.

Fig. 25 shows the comparison of these sensitivity coefficients as functions of R_H for three representative lean, stoichiometric and rich cases. It is seen that for all ϕ_F, the kinetic term is the largest sensitivity factor in increasing the burning flux. The sensitivity factor for the thermal effect is smaller, but nevertheless still significant, while the factor for the diffusion effect is substantially smaller and can also assume negative values for lean mixtures. Furthermore, all three sensitivity factors at the stoichiometric condition assume values one order smaller than those at off-stoichiometric conditions of $\phi_F = 0.6$ and 1.4. This corroborates the earlier result that laminar flame speed shows the weakest

dependence on R_H at near stoichiometric condition [103]. Further computations of other hydrocarbons showed that the above flame speed dependence on R_H holds for methane, ethane, and propane, indicating that there exists the possibility of generalizing the phenomena.

5.2. Flame front stability

Accurate determination of laminar burning velocity is always counteracted by the presence of cells over the flame surface, which increases the flame surface area and consequently enhances the flame propagation speed [142], especially at high pressures and/or for lean hydrogen or light hydrocarbon flames and rich heavy hydrocarbon flames. The flame front cellular instability-induced self-acceleration and the subsequent self turbulization, and even transition to detonation [143], could potentially promote engine knock [144,145]. For this reason, cellular instability has raised a significant amount of attention.

Three mechanisms of cellular instability are well established: hydrodynamic instability [146,147], diffusional-thermal instability [104,148,149], and instability resulting from the body force [150]. The body force induced – or the so-called Rayleigh–Taylor instability – is conspicuous when the flame speed is decreased, because growth rate is strongly dependent on the flame speed [11]. Hydrodynamic instability was first recognized theoretically in 1938 by Darrieus [146], and later in 1944, it was predicted independently by Landau [147]. They assumed that the flame was a thin interface of density discontinuity propagating towards the unburned mixture at a constant speed, the growth rate of the hydrodynamic disturbance is proportional to the thermal expansion ratio and thus the hydrodynamic instability is strongly dependent on the thermal expansion ratio and flame thickness. It should be noted that no length scale was embedded in the Darrieus–Landau theory, thus the flame was unconditionally unstable to all wavelengths of hydrodynamic disturbances. Clanet and Searby [151] established a perfectly planar laminar flame with an acoustic re-stabilization technique, as shown therein. They were among the first to experimentally measure the growth rate of Darrieus–Landau instability and their observed image was given in Fig. 26.

For mixtures in which the deficient reactant is also the constituent of the largest diffusivity, the formation of cells was observed for both plane flame [148], as shown in Fig. 27, and spherical flame [104], as shown in Fig. 28(b). The cellularity in such cases is a consequence of a diffusional-thermal instability, which results from the competing effects of heat conduction from the flame and reactant diffusion towards the flame [149,152,153]. Lewis number (*Le*) is defined as the ratio of heat diffusivity of the mixture to mass diffusivity of the limiting reactant. When Le is below some critical value, *Le** (slightly lower than unity), diffusional-thermal instability could be observed during the initial phase of propagation, i.e., the flame radius is the order of flame thickness [152].

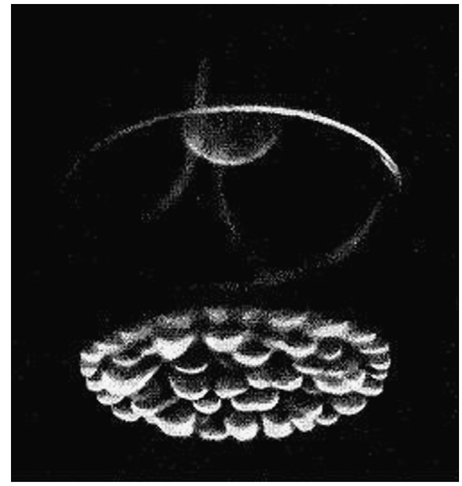


Fig. 27. Images of fully developed cell structure for rich propane/air flame [148].

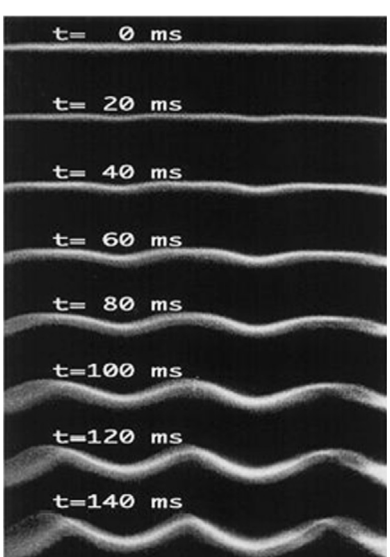


Fig. 26. Images from high speed film of growth of instability [151]. Framing rate of 500 images/s, wave length of 2 cm and laminar flame speed of 11.5 cm /s.

Obviously for mixtures not apart from stoichiometry, the formation of cells on the flame surface results from the combined influence of the hydrodynamic and diffusional-thermal instabilities. The opposite nonequidiffusive behavior of heavy hydrocarbon (propane, for instance)/air and hydrogen/air was well established [138,154]. However, there are limited reports on the cell formation of hydrogen enriched hydrocarbon flames, especially at high pressures where the hydrodynamic instability mechanism is conspicuous.

Rayleigh–Taylor instability is conspicuous only when the flame speed is very low, thus the effect of hydrogen addition tends to prohibit this instability mechanism because the addition of hydrogen will increase the laminar flame speed.

Law and Kwon [128] studied the propane substituted hydrogen/air flame at atmospheric pressure and found that the flame front instability of the lean hydrogen air flame is progressively moderated, or diminished, as SFHC increases; this is clearly shown from the flame images (as shown in Fig. 28(a)). Other results of Law et al. [135] and Tang et al. [155] were also shown in the figure. The propane substitution extent parameter SFHC and the propane mixing ratio α are all converted to the simply understanding hydrogen percentage X_{H2}, as tabulated at the bottom, or on the right, of each series of images. It is expected that both the diffusional-thermal instability and the hydrodynamic instability were prohibited with increasing SFHC, α or decreasing X_{H2}, respectively in Ref. [128,135,155], due to suppression of diffusional-thermal cells and the substantial increase of flame thickness, as more propane is present in the mixture. The Lewis number (which accounts for the thermal-diffusion effect) is conventionally estimated for sufficiently off-stoichiometric mixtures from the free stream values of the mixture transport properties. For blends of fuel with different transport properties, however, the Lewis number should be a global flame parameter, evaluated through flame response or with specific weighted averaging. As shown in

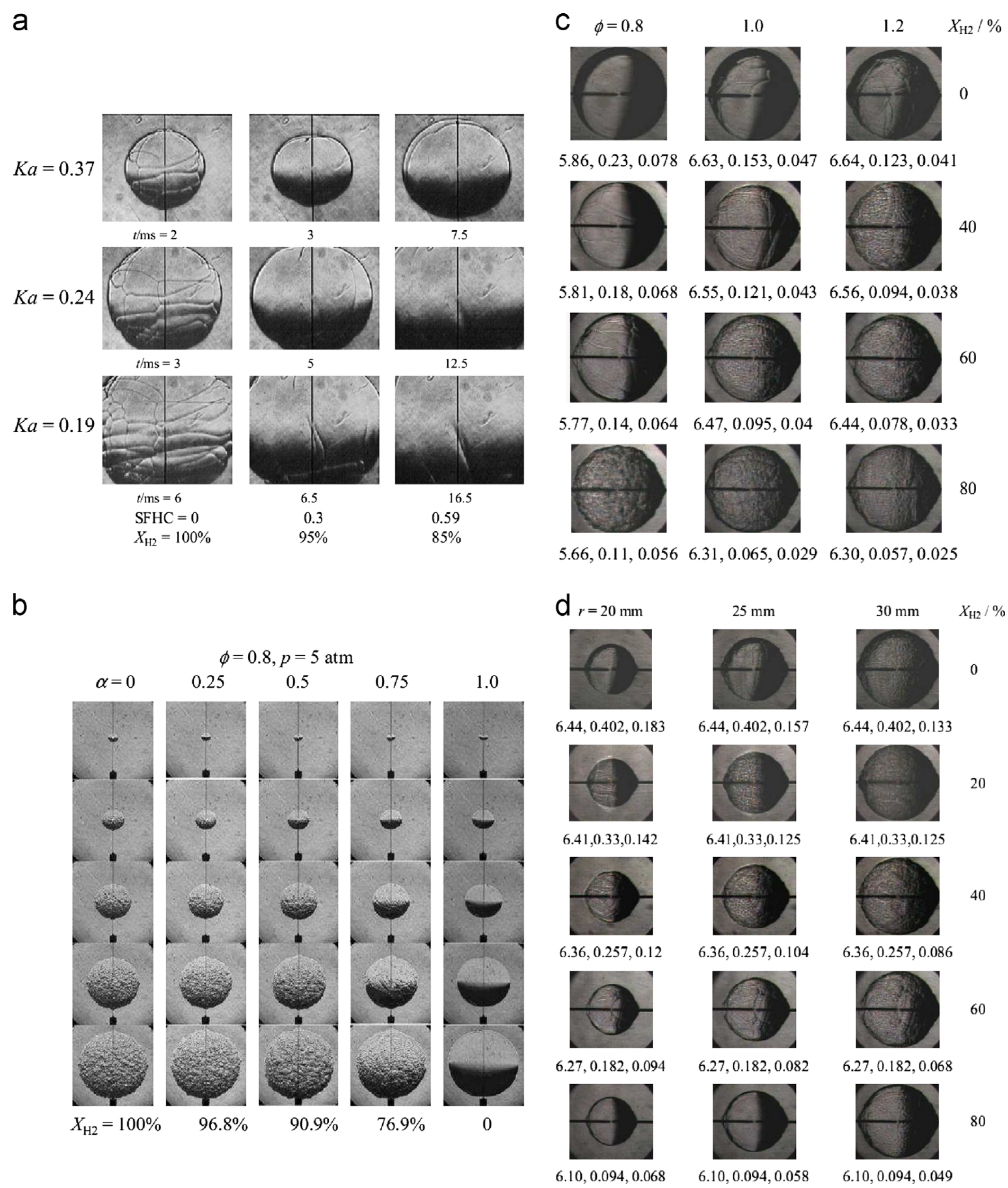


Fig. 28. Schlieren photographs: (a) C_3H_8-substituted H_2–air (ϕ=0.6 at NTP). Ref. [128]. (b) Hydrogen, hydrogen/propane (propane mixing ratio =0.25, 0.5 and 0.75) and propane in air at 5 atm. Adapted from Ref. [135]. (c) Lean (ϕ=0.8), stoichiometric and moderately rich (ϕ=1.2) propane/hydrogen mixtures at 5 atm (σ, δ, mm, Ka). Adapted from Ref. [155]. (d) Adequately rich (ϕ=1.4) propane/hydrogen mixtures at 5 atm. Adapted from Ref. [155].

Fig. 29(a), the flame Lewis number is decreased with the increase of X_{H2} (decreasing propane mixing ratio α), indicating the thermal-diffusionally de-stabilizing effect of hydrogen addition.

For the rich flames, the effect of propane substitution is not clear because both the flame thickness and the density ratio increase substantially as the SFHC increases. The rich hydrogen/air flames are thermal-diffusionally stable and thus Law and Kwon concluded that increasing propane would not likely promote flame front instability; however, their images were taken at atmospheric pressure, where the hydrodynamic instability effect is not as strong. Another series of Schlieren images by Law et al. [135] was taken at higher pressures, but no results of fuel rich conditions were presented therein.

Tang et al. [155] showed that for adequately rich propane/air flame, the net effect of adding hydrogen to flame front instability depends on the competition between the thermal-diffusion mechanism and the hydrodynamic mechanism, and they did observe that the flame front was first destabilized, then stabilized with the increase of the hydrogen addition, as shown in Fig.28(d). For X_{H2} less than 40%, although the Lewis number increases (as shown in Fig. 29(b)), and thus the thermal-diffusion effect tends to stabilize the flame; flame front instability is still promoted because of the hydrodynamic destabilizing effect due to the significant decrease in flame thickness (δ_l). However, for X_{H2} larger than 40%, the Lewis number increases more significantly and the flame tends to be stabilized as X_{H2} increases. This implies the dominant influence of the Lewis number compared to those of other parameters, such as σ, δ_l, and Ka. The non-monotonic behavior at fuel rich conditions indicates that there exists a mixture composition (X_{H2}=40%), at which the flame is the most unstable due to the combination of effects of the hydrodynamic and diffusional-thermal instabilities.

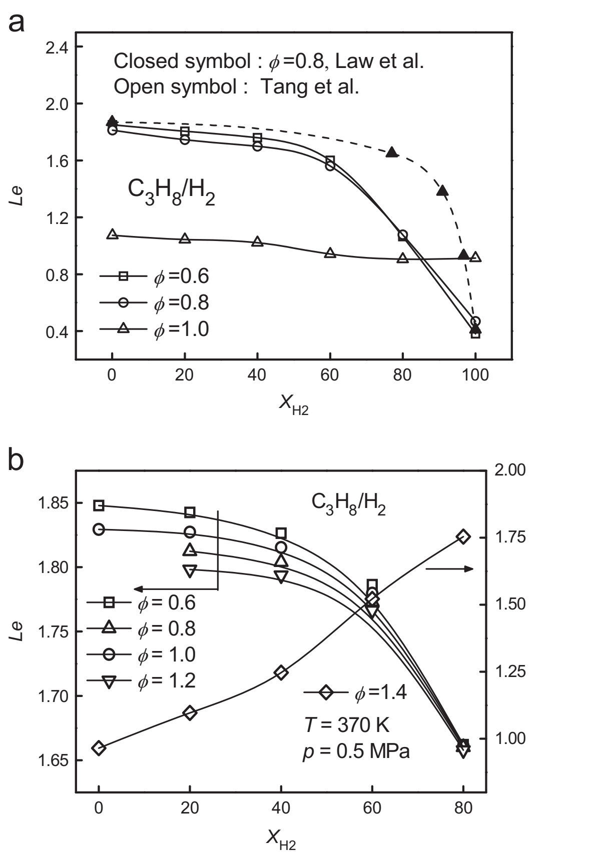


Fig. 29. Global flame Lewis number for propane/hydrogen/air mixture as a function of X_{H2}. (a) Evaluated from flame response, Refs. [102,135]. (b) Weighted average value [155].

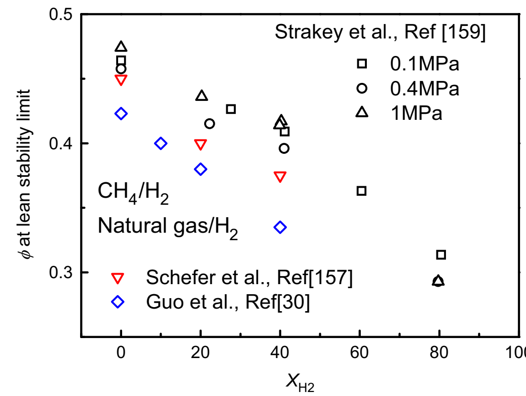


Fig. 30. Lean stability limit data of hydrogen enriched flames. Data obtained from Strakey et al. [159] (swirl-stabilized burner for H_2+natural gas, squares (□): 1 atm; circles (○): 4 atm; up triangles (△): 10 atm); Schefer [157] (swirl-stabilized burner for H_2+methane at 1 atm, down triangles, ▽), and Guo et al. [30] (counter-flow flames of H_2+methane at 1 atm, diamond, ◇).

6. Effects of hydrogen addition on lean premixed combustion

Operating an engine with excess air, under lean conditions, has significant benefits in terms of increased engine efficiency and reduced emissions. However, under high dilution levels, a lean limit is reached in which combustion becomes unstable, significantly deteriorating drivability and engine efficiency and limiting the full potential of lean combustion. Due to the high laminar flame speed of hydrogen, adding a hydrogen-rich mixture with gasoline into the engine helps to stabilize combustion, extending the lean limit.

Lean premixed combustion (LPC) is also conceptually advantageous in gas turbines due to its lower flame temperature, which results in less thermal load and lower emission of NO_x. However, LPC is susceptible to combustion instabilities because of the weak burning and extinction caused by local stretching and heat loss [156]. One approach to solving the combustion stability problem of LPC is through the addition of H_2, because hydrogen can sustain vigorous burning at relatively lower temperatures compared to hydrocarbon [95].

6.1. Swirl stablized lean premixed combustion

There have been several studies of the effects of hydrogen addition on the lean stability limit of swirl-stabilized premixed flames [157–159] and stagnation flames [30,156]. These works demonstrated a significant extension of the lean stability limit by the addition of hydrogen.

Strakey et al. [159] measured the lean blowout equivalence ratio of natural gas and air mixtures with a hydrogen addition in a swirl-stabilized burner; they found that when the hydrogen concentration X_{H2} in the fuel mixtures is increased from 0 to 80%, the lean blowout equivalence ratio is reduced from $\phi\sim0.46$ to $\phi\sim0.30$. Additionally, their experimental data indicated that at different pressures the lean stability limit is insensitive to a variation of pressure. Schefer [157] investigated stability characteristics of premixed, swirl-stabilized methane air flames with emphasis on the effect of a hydrogen addition. It is seen in Fig. 30 that Schefer's measurement is slightly lower than that of Strakey et al. This might be caused by the hydrocarbon compositions in the natural gas.

Guo et al. [30] measured the extinction limit of premixed counter-flowing methane air flames with a hydrogen addition of up to 40%; the extinction limit was also included in Fig. 30. It is seen that Guo's measurement is lower than that of Schefer and Strakey et al., which is reasonable because an unstable flame could be extinguished by decreasing the equivalence ratio. Overall, the extension of the lean stability limit by the addition of hydrogen is well illustrated by Fig. 30. The extinction strain rate of hydrogen enriched lean premixed methane flames in highly strained counter-flowing fields has been experimentally and numerically investigated by Jackson et al. [160]; they experimentally observed that, with the increase of hydrogen concentration in the fuel blends, the extinction strain rate is significantly reduced.

6.2. Pollutant emissions

Hydrogen addition can significantly reduce the emission of CO. However, one concern about adding hydrogen into hydrocarbon is the increase of flame temperature, which may result in higher emissions of NO_x. Schefer et al. [158] investigated the pollutant emissions from the swirl-stabilized lean premixed natural gas combustion with and without the addition of hydrogen. Fig. 31 shows the radial profile of CO and NO_x emissions at the axial plane of $z=5.1$ and 20.3 cm. It is seen that in the central region, the CO emissions at both axial planes from natural gas combustion range from 15 to 100 ppm, while the hydrogen enriched flames produce CO values of less than 10 ppm. Fig. 31(b) shows that the NO_x concentration from hydrogen enriched natural gas combustion is higher than that from pure natural gas. This is because the combustion of natural gas requires longer residence distance than the hydrogen enriched flames in order to reach steady NO_x concentration because of faster combustion of with hydrogen. At $z=20.3$, steady NO_x concentration is reached, as shown in Fig. 31(d), and both fuels emit similar level of NO_x. These results demonstrate that a significant reduction in CO emissions is

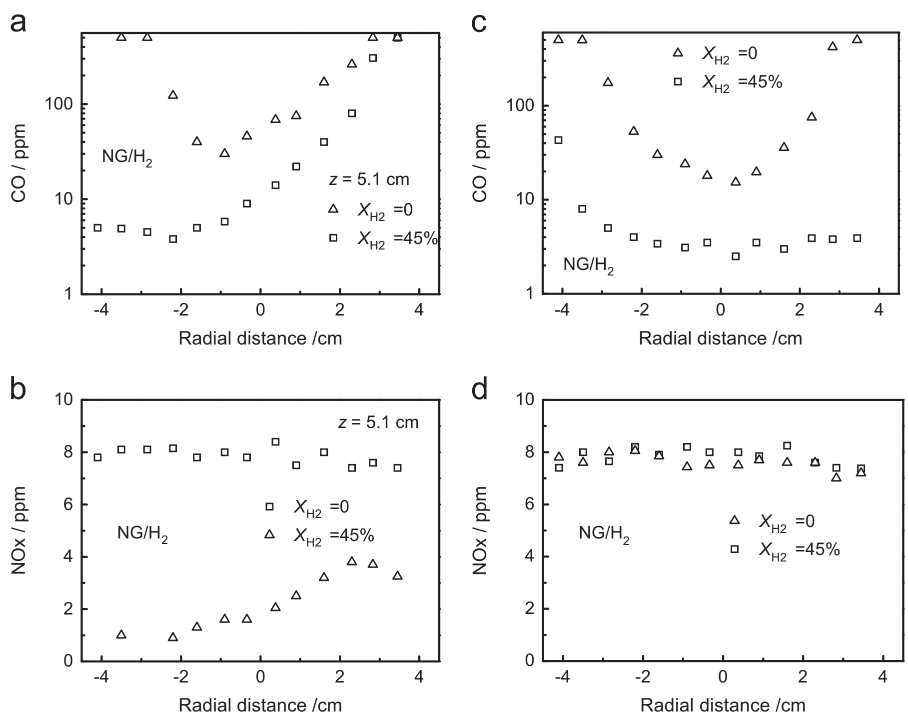


Fig. 31. CO and NO_x concentration profiles in the radial direction. Measurements at plane $z=5.1$ and 20.3 cm. Adapted from Schefer et al. [158].

realized by hydrogen addition without adversely affecting the NO_x emissions.

7. Concluding remarks

Increasingly unavailable fossil fuels and greenhouse gas emissions from transportation vehicles are driving investigations of alternative fuels. Among them, hydrogen offers the greatest potential benefit to the environment and energy supply. Hydrogen is the most abundant element in the universe; it is a versatile energy carrier that can be made from a variety of primary energy sources such as natural gas, coal, and biomass, and non-carbon energy sources such as solar, nuclear, hydroelectric, and wind. Hydrogen can burn with high efficiency and produce essentially zero emissions. However, attractive as it is, a hydrogen economy is challenged by technical, economical and infrastructural barriers. For instance, there are significant difficulties associated with hydrogen storage due to its high flammability limits, low ignition energy (which causes safety problems), and its low volumetric energy content, which requires extra energy for high pressure storage. Additionally, there exists some unresolved issues for pure H_2 combustion, such as knock, detonation, pre-ignition, and flashback. For these reasons, fossil fuels still dominate the current primary energy supply. To bridge this situation, a more rational approach is to use hydrogen/hydrocarbon fuel blends, which synergistically resolve storage and combustion problems associated with burning pure hydrogen or pure hydrocarbons.

In this work, recent progress in the fundamental investigations on the combustion characteristics of hydrogen/hydrocarbon fuel blends has been reviewed. Experimental results show that the flammability limits of hydrocarbon are extended with the addition of hydrogen. Also Le Chatelier's Rule can predict the dependence of a lower flammability limit with reasonable accuracy. The minimum ignition energy of hydrogen/hydrocarbon blends shows a power-law dependence on the quenching distance and both decrease significantly with the increased hydrogen fraction X_{H2}. Ignition of methane and air stream in a supersonic mixing layer is promoted with hydrogen addition because of the accelerated production of H and O radicals. Non-premixed ignition temperatures in counter-flowing methane vs. hot air streams are decreased significantly with a small amount of hydrogen, and this effect is moderated as hydrogen concentration is increased to 7% and the effect of hydrogen addition effect disappears when the hydrogen fraction is higher than 30%.

Auto-ignition of hydrogen enriched hydrocarbons by shock-waves has been reviewed in detail. With an increase of the hydrogen fraction, ignition behavior of hydrogen/hydrocarbon fuel blends in Argon-diluted oxygen exhibits three distinct behaviors. For a hydrogen fraction less than 40%, the dependence of ignition delay time on pressure and equivalence ratio resembles that of pure hydrocarbon and ignition is dominated by methane chemistry. For a hydrogen fraction higher than 80%, the dependence of the ignition delay time on pressure and equivalence ratio resembles that of pure hydrogen and ignition is dominated by hydrogen chemistry. For a hydrogen fraction in the range between 40% and 80%, ignition delay time dependence on pressure and equivalence ratio resembles neither hydrogen nor hydrocarbon, and ignition is governed by the combined chemistry of hydrogen and hydrocarbon.

The laminar flame speed of hydrogen/hydrocarbon fuel blends is found to exhibit three behavior regimes. When X_{H2} increases, the laminar flame speed of the fuel blend increases, but the increment is small; the increment becomes significant when X_{H2} is higher than about 40%. When X_{H2} is further increased to more than 80%, the laminar flame speed of the mixture increases even more substantially. When a specifically defined hydrogen addition parameter R_H is defined, the flame speed of *n*-butane/hydrogen is found to increase linearly with R_H due to altered thermodynamics, diffusivity, and chemical kinetics with hydrogen addition. Additionally, the effect of hydrogen is minimized at around the stoichiometric condition. Computation with other fuels such as methane, ethene, and propane showed that the laminar flame speed dependence on R_H is generous for these hydrocarbons.

There are three mechanisms that influence flame front instability behavior: the body-force effect, the hydrodynamic effect and the thermal-diffusion effect.

Hydrogen addition will reduce the body-force effect because of increased flame speed. For lean heavy hydrocarbons (C3 or higher), a hydrogen addition will decrease the overall Lewis number, resulting in a promoted thermal-diffusional instability. While for sufficiently rich heavy hydrocarbons, thermal-diffusional instability tends to be inhibited by the addition of hydrogen. Hydrodynamic instability is promoted by the increase of hydrogen because of the decreased flame thickness. A hydrogen addition increases the resistance to the strain rate, leading to an extended lean stability limit and better stabilized swirl burner combustion. Additionally, a significant reduction in CO emissions is realized by the addition of hydrogen, without adversely affecting the NO_x emissions.

Acknowledgments

This work is supported by the National Natural Science Foundation of China (51136005 and 51121092). Support from the Fundamental Research Funds for the Central Universities is also appreciated.

References

[1] Ogden JM. Hydrogen: the fuel of the future? Phys Today 2002;55:69–75.
[2] Mariño F, Boveri M, Baronetti G, Laborde M. Hydrogen production from steam reforming of bioethanol using Cu/Ni/K/γ–Al_2O_3 catalysts. Effect of Ni. Int J Hydrog Energy 2001;26:665–8.
[3] Crabtree GW, Dresselhaus MS, Buchanan MV. The hydrogen economy. Phys Today 2004;57:39–44.
[4] Satyapal S, Read C, Ordaz G, Thomas G. US Department of Energy Hydrogen Program Annual Merit Review Proceedings; 2006.
[5] de la Casa-Lillo MA, Lamari-Darkrim F, Cazorla-Amorós D, Linares-Solano A. Hydrogen storage in activated carbons and activated carbon fibers. J Phys Chem B 2002;106:10930–4.
[6] Dillon AC, Jones KM, Bekkedahl TA, Kiang CH, Bethune DS, Heben MJ. Storage of hydrogen in single-walled carbon nanotubes. Nature 1997;386:377–9.
[7] Coward HF, Jones GW. Limits of flammability of gases and vapors. Mines Bo Bulletin 503; 1952. Washington DC.
[8] Zabetakis MG. Flammability characteristics of combustible gases and vapors. Bulletin 627; 1965. Pittsburgh.
[9] Kuchta JM. Investigation of fire and explosion accidents in the chemical, mining and fuel-related industries. Mines Bo Bulletin 680; 1985. Pittsburgh.
[10] Cashdollar KL, Zlochower I A, Green GM, Thomas RA, Hertzberg M. Flammability of methane, propane, and hydrogen gases. J Loss Prev Process Ind 2000;13:327–40.
[11] Cashdollar KL, Hertzberg M. 20-l explosibility test chamber for dusts and gases. Rev Sci Instr 1985;56:596–602.
[12] Hertzberg M, Cashdollar KL, Zlochower IA. Flammability limit measurements for dusts and gases: ignition energy requirements and pressure dependences. In: Symposium (international) on combustion, vol. 21; 1988. p. 303–13.
[13] Ju YG, Guo HS, Maruta K, Niioka T. Determination of burning velocity and flammability limit of methane/air mixture using counterflow flames. Jpn J Appl Phys 1999;38:961–7.
[14] ASTM. Standard test for concentration limits of flammability of chemicals; 2001.
[15] ASTM. Standard test for limiting oxygen (oxidant) concentration in gases and vapors; 2001.
[16] ASTM. Standard practice for determining limits of flammability of chemicals at elevated temperature and pressure; 1999.
[17] Van den Schoor F, Hermanns RTE, van Oijen JA, Verplaetsen F, de Goey LPH. Comparison and evaluation of methods for the determination of flammability limits, applied to methane/hydrogen/air mixtures. J Hazard Mater 2008;150:573–81.
[18] Schröder V, Daubitz R. Evaluation of standard test methods for the determination of explosion limits of gases and vapors. In: Loss prenvention symposium. Prague, Czech; 2004.
[19] Ju YG, Masuya G, Ronney PD. Effects of radiative emission and absorption on the propagation and extinction of premixed gas flames. In: Symposium (international) on combustion; 1998. p. 2619–26.
[20] Lakshmisha KN, Paul PJ, Mukunda HS. On the flammability limit and heat loss in flames with detailed chemistry; 1990.
[21] Sibulkin M, Frendi A. Prediction of flammability limit of an unconfined premixed gas in the absence of gravity. Combust Flame 1990;82:334–45.
[22] Buckmaster J, Mikolaitis D. A flammability-limit model for upward propagation through lean methane/air mixtures in a standard flammability tube. Combust Flame 1982;45:109–19.
[23] Bui-Pham MN, Miller JA. Rich methane/air flames: burning velocities, extinction limits, and flammability limit. In: Symposium (international) on combustion, vol. 25; 1994. p. 1309–15.
[24] Burgess MJ, Wheeler RV. The lower limit of inflammation of mixtures of the paraffin hydrocarbons with air. J Chem Soc 1911;99:2013–30.
[25] Law CK. Combustion physics. New York: Cambridge University Press; 2006.
[26] Law CK, Egolfopoulos FN. A unified chain-thermal theory of fundamental flammability limits. In: Symposium (international) on combustion, vol. 24; 1992. p. 137–44.
[27] Wierzba I, Ale BB. Rich flammability limits of fuel mixtures involving hydrogen at elevated temperatures. Int J Hydrog Energy 2000;25:75–80.
[28] Shoshin YL, Goey LPHd. Experimental study of lean flammability limits of methane/hydrogen/air mixtures in tubes of different diameters. Exp Thermal Fluid Sci 2010;34:373–80.
[29] Miao H, Lu L, Huang Z. Flammability limits of hydrogen-enriched natural gas. Int J Hydrog Energy 2011;36:6937–47.
[30] Guo HS, Smallwood GJ, Liu FS, Ju YG, Gulder OL. The effect of hydrogen addition on flammability limit and NO_x emission in ultra-lean counterflow CH4/air premixed flames. In: Proceedings of the combustion institute, vol. 30; 2005. p. 303–11.
[31] Lewis B, Von Elbe G. Combustion, flames and explosion of gases. London: Harcourt Brace Jovanovich Publishers; 1987.
[32] Williams FA. Combustion theory. Menlo Park, CA: The Benjamin/Cummings Publishing Company, Inc; 1985.
[33] Calcote HF, Gregory CA, Barnett CM, Gilmer RB. Spark ignition. Effect of molecular structure. Ind Eng Chem 1952;44:2656–62.
[34] Glassman I. Combustion. second ed.. New York: Academic Press, Inc;; 1987.
[35] Hankinson G, Mathurkar H, Lowesmith BJ. Ignition energy and ignition probability of methane–hydrogen–air mixtures. In: Internationl conference on hydrogen safety; 2009.
[36] Fukuda M, Korematsu K, Sakamoto M. On quenching distance of mixtures of methane and hydrogen with air. Bull Jpn Soc Mech Eng 1981;24:1192–7.
[37] He L. Critical conditions for spherical flame initiation in mixtures with high Lewis numbers. Combust Theory Model 2000:4.
[38] Chen Z, Ju Y. Theoretical analysis of the evolution from ignition kernel to flame ball and planar flame. Combust Theory Model 2007;11:427–53.
[39] Kelley AP, Jomaas G, Law CK. Critical radius for sustained propagation of spark-ignited spherical flames. Combust Flame 2009;156:1006–13.
[40] Nishioka M, Law CK. A numerical study of ignition in the supersonic hydrogen/air laminar mixing layer. Combust Flame 1997;108:199–219.
[41] Ju Y, Niioka T. Reduced kinetic mechanism of ignition for nonpremixed hydrogen/air in a supersonic mixing layer. Combust Flame 1994;99:240–6.
[42] Treviño C, Méndez F. Reduced kinetic mechanism for methane ignition. In: Symposium (international) on combustion, vol. 24; 1992. p. 121–7.
[43] Tokuhashi K, Horiguchi S, Urano Y, Iwasaka M, Ohtani H, Kondo S. Premixed silane–oxygen–nitrogen flames. Combust Flame. 1990;82:40–50.
[44] Bier K, Kappler G, Wilhelmi H. Experiments on the combustion of hydrogen and methane injected transversely into a supersonic air stream. In: Symposium (international) on combustion, vol. 13; . 1971. p. 675–82.
[45] Ju Y, Niioka T. Ignition simulation of methane/hydrogen mixtures in a supersonic mixing layer. Combust Flame 1995;102:462–70.
[46] Balakrishnan G, Smooke MD, Williams FA. A numerical investigation of extinction and ignition limits in laminar nonpremixed counterflowing hydrogen–air streams for both elementary and reduced chemistry. Combust Flame 1995;102:329–40.
[47] Kreutz TG, Law CK. Ignition in nonpremixed counterflowing hydrogen versus heated air: computational study with detailed chemistry. Combust Flame 1996;104:157–75.
[48] Kreutz TG, Law CK. Ignition in nonpremixed counterflowing hydrogen versus heated air: computational study with skeletal and reduced chemistry. Combust Flame 1998;114:436–56.
[49] Kreutz TG, Nishioka M, Law CK. The role of kinetic versus thermal feedback in nonpremixed ignition of hydrogen versus heated air. Combust Flame 1994;99:758–66.
[50] Zheng XL, Law CK. Ignition of premixed hydrogen/air by heated counterflow under reduced and elevated pressures. Combust Flame 2004;136:168–79.
[51] Zheng XL, Blouch JD, Zhu DL, Kreutz TG, Law CK. Ignition of premixed hydrogen/air by heated counterflow. In: Proceedings of the combustion institute, vol. 29; 2002. p. 1637–43.
[52] Fotache CG, Kreutz TG, Law CK. Ignition of counterflowing methane versus heated air under reduced and elevated pressures. Combust Flame 1997;108:442–70.
[53] Fotache CG, Wang H, Law CK. Ignition of ethane, propane, and butane in counterflow jets of cold fuel versus hot air under variable pressures. Combust Flame 1999;117:777–94.
[54] Fotache CG, Kreutz TG, Law CK. Ignition of hydrogen-enriched methane by heated air. Combust Flame 1997;110:429–40.
[55] Kim TJ, Yetter RA, Dryer FL. New results on moist CO oxidation: high pressure, high temperature experiments and comprehensive kinetic modeling. In: Symposium (international) on combustion, vol. 25; 1994. p. 759–66.

[56] Frenklach M, Wang H, Yu CL, Goldenberg M, Bowman CT, Hanson RK, et al. An optimized detailed chemical reaction mechanism for methane combustion 1995.
[57] Gersen S, Anikin N, Mokhov A, Levinsky H. Ignition properties of methane/hydrogen mixtures in a rapid compression machine. Int J Hydrog Energy 2008;33:1957–64.
[58] Spadaccini LJ, Colket MB. Ignition delay characteristics of methane fuels. Prog Energy Combust Sci 1994;20:431–60.
[59] Gokulakrishnan P, Gaines G, Currano J, Klassen MS, Roby RJ. Experimental and kinetic modeling of kerosene-type fuels at gas turbine operating conditions. J Eng Gas Turbines Power 2007;129:655–63.
[60] Holton MM, Gokulakrishnan P, Klassen MS, Roby RJ, Jackson GS. Autoignition delay time measurements of methane, ethane, and propane pure fuels and methane-based fuel blends. J Eng Gas Turbines Power 2010;132:091502.
[61] Curran HJ, Gaffuri P, Pitz WJ, Westbrook CK. A comprehensive modeling study of *n*-heptane oxidation. Combust Flame 1998;114:149–77.
[62] Pitz WJ, Naik CV, Mhaoldúin TN, Westbrook CK, Curran HJ, Orme JP, et al. Modeling and experimental investigation of methylcyclohexane ignition in a rapid compression machine. In: Proceedings of the combustion institute, vol. 31; 2007. p. 267–75.
[63] Burcat A, Scheller K, Lifshitz A. Shock-tube investigation of comparative ignition delay times for C1–C5 alkanes. Combust Flame 1971;16:29–33.
[64] Ciezki HK, Adomeit G. Shock-tube investigation of self-ignition of *n*-heptane–air mixtures under engine relevant conditions. Combust Flame 1993;93:421–33.
[65] Zhang Y, Huang Z, Wei L, Zhang J, Law CK. Experimental and modeling study on ignition delays of lean mixtures of methane, hydrogen, oxygen, and argon at elevated pressures. Combust Flame 2012;159:918–31.
[66] Dryer FL, Chaos M. Ignition of syngas/air and hydrogen/air mixtures at low temperatures and high pressures: experimental data interpretation and kinetic modeling implications. Combust Flame 2008:152.
[67] Heufer K, Olivier H. Determination of ignition delay times of different hydrocarbons in a new high pressure shock tube. Shock Waves 2010;20: 307–16.
[68] Pang G, Davidson D, Hanson R. Experimental study and modeling of shock tube ignition delay times for hydrogen–oxygen–argon mixtures at low temperatures. In: Proceedings of the combustion institute, vol. 32; 2009. p. 181–8.
[69] Petersen E, Davidson D, Hanson R. Kinetics modeling of shock-induced ignition in low-dilution CH4/O2 mixtures at high pressures and intermediate temperatures. Combust Flame 1999;117:272–90.
[70] Petersen E, Davidson D, Röhrig M, Hanson R. High-pressure shock-tube measurements of ignition times in stoichiometric H_2/O_2/AR mixtures. In: Proceedings of the 20th international symposium on shock waves; 1996. p. 941–946.
[71] Petersen EL, Davidson DF, Hanson RK. Ignition delay times of ram accelerator CH_4/O_2/diluent mixtures. J Propuls Power 1999;15:82–91.
[72] Petersen EL, Hall JM, Smith SD, de Vries J, Amadio AR, Crofton MW. Ignition of lean methane-based fuel blends at gas turbine pressures. J Eng Gas Turbines Power 2007;129:937.
[73] Petersen EL, Kalitan DM, Barrett AB, Reehal SC, Mertens JD, Beerer DJ, et al. New syngas/air ignition data at lower temperature and elevated pressure and comparison to current kinetics models. Combust Flame 2007;149: 244–7.
[74] Petersen EL, Rickard MJA, Crofton MW, Abbey ED, Traum MJ, Kalitan DM. A facility for gas-and condensed-phase measurements behind shock waves. Meas Sci Technol 2005;16:1716.
[75] Petersen EL, Röhrig M, Davidson DF, Hanson RK, Bowman CT. High-pressure methane oxidation behind reflected shock waves. In: Proceedings of the combustion institute; 1996. Elsevier, p. 799–806.
[76] Herzler J, Naumann C. Shock-tube study of the ignition of methane/ethane/hydrogen mixtures with hydrogen contents from 0% to 100% at different pressures. In: Proceedings of the combustion institute, vol. 32; 2009. p. 213–20.
[77] Li J, Zhao Z, Kazakov A, Dryer FL. An updated comprehensive kinetic model of hydrogen combustion. Int J Chem Kinet 2004;36:566–75.
[78] Konnov A. Refinement of the kinetic mechanism of hydrogen combustion. Khim Fiz 2004;23:5–18.
[79] Lifshitz A, Scheller K, Burcat A, Skinner GB. Shock-tube investigation of ignition in methane–oxygen–argon mixtures. Combust Flame 1971;16:311–21.
[80] Cheng R, Oppenheim A. Autoignition in methane–hydrogen mixtures. Combust Flame 1984;58:125–39.
[81] de Vries J, Petersen E. Autoignition of methane-based fuel blends under gas turbine conditions. In: Proceedings of the combustion institute, vol. 31; 2007. p. 3163–71.
[82] Huang J, Bushe W, Hill P, Munshi S. Experimental and kinetic study of shock initiated ignition in homogeneous methane–hydrogen–air mixtures at engine—relevant conditions. Int J Chem Kinet 2006;38:221–33.
[83] Chaumeix N, Pichon S, Lafosse F, Paillard CE. Role of chemical kinetics on the detonation properties of hydrogen/natural gas/air mixtures. Int J Hydrog Energy 2007;32:2216–26.
[84] Grillo A, Slack M. Shock tube study of ignition delay times in methane–oxygen–nitrogen–argon mixtures. Combust Flame 1976;27:377–81.
[85] Seery DJ, Bowman CT. An experimental and analytical study of methane oxidation behind shock waves.* Combust Flame 1970;14:37–47.
[86] Huang J, Hill P, Bushe W, Munshi S. Shock-tube study of methane ignition under engine-relevant conditions: experiments and modeling. Combust Flame 2004;136:25–42.
[87] Skinner GB, Ringrose GH. Ignition delays of a hydrogen–oxygen–argon mixture at relatively low temperatures. J Chem Phys 1965;42:2190.
[88] Aung KT, Hassan MI, Faeth GM. Flame stretch interactions of laminar premixed hydrogen/air flames at normal temperature and pressure. Combust Flame 1997;109:1–24.
[89] Westbrook CK, Dryer FL. Simplified reaction-mechanisms for the oxidation of hydrocarbon fuels in flames. Combust Sci Technol 1981;27:31–43.
[90] Westbrook CK, Dryer FL. Chemical kinetic modeling of hydrocarbon combustion. Prog Energy Combust Sci 1984;10:1–57.
[91] Milton BE, Keck JC. Laminar burning velocities in stoichiometric hydrogen and hydrogen–hydrocarbon gas mixtures. Combust Flame 1984;58:13–22.
[92] Magnussen BF, Hjertager BH. On mathematical modeling of turbulent combustion with special emphasis on soot formation and combustion. In: Symposium (international) on combustion, vol. 16; 1977. p. 719–29.
[93] Veynante D, Vervisch L. Turbulent combustion modeling. Prog Energy Combust Sci 2002;28:193–266.
[94] Peters N. Turbulent combustion. New York: Cambridge University Press; 2000.
[95] Yu G, Law CK, Wu CK. Laminar flame speeds of hydrocarbon + air mixtures with hydrogen addition. Combust Flame 1986;63:339–47.
[96] Bosschaart KJ, de Goey LPH. Detailed analysis of the heat flux method for measuring burning velocities. Combust Flame 2003;132:170–80.
[97] Bosschaart KJ, de Goey LPH, Burgers JM. The laminar burning velocity of flames propagating in mixtures of hydrocarbons and air measured with the heat flux method. Combust Flame 2004;136:261–9.
[98] Bradley D, Hicks RA, Lawes M, Sheppard CGW, Woolley R. The measurement of laminar burning velocities and markstein numbers for *iso*-octane–air and *iso*-octane–*n*-heptane–air mixtures at elevated temperatures and pressures in an explosion bomb. Combust Flame 1998;115:126–44.
[99] Bradley D, Lawes M, Liu K, Verhelst S, Woolley R. Laminar burning velocities of lean hydrogen–air mixtures at pressures up to 1.0 MPa. Combust Flame 2007;149:162–72.
[100] Huang Z, Zhang Y, Zeng K, Liu B, Wang Q, Jiang D. Measurements of laminar burning velocities for natural gas–hydrogen–air mixtures. Combust Flame 2006;146:302–11.
[101] Tang CL, He JJ, Huang ZH, Jin C, Wang JH, Wang XB, et al. Measurements of laminar burning velocities and Markstein lengths of propane–hydrogen–air mixtures at elevated pressures and temperatures. Int J Hydrog Energy 2008;33:7274–85.
[102] Tang CL, Huang ZH, Jin C, He JJ, Wang JH, Wang XB, et al. Laminar burning velocities and combustion characteristics of propane–hydrogen–air premixed flames. Int J Hydrog Energy 2008;33:4906–14.
[103] Tang CL, Huang ZH, Law CK. Determination, correlation, and mechanistic interpretation of effects of hydrogen addition on laminar flame speeds of hydrocarbon–air mixtures. In: Proceedings of the combustion institute, vol. 33; 2011. p. 921–8.
[104] Manton J, von Elbe G, Lewis B. Nonisotropic propagation of combustion waves in explosive gas mixtures and the development of cellular flames. J Chem Phys 1952;20:153–7.
[105] Palm-Leis A, Strehlow RA. On the propagation of turbulent flames. Combust Flame 1969;13:111–29.
[106] Lamoureux N, Djebaili-Chaumeix N, Paillard CE. Laminar flame velocity determination for H-2–air–He–CO_2 mixtures using the spherical bomb method. Exp Thermal Fluid Sci 2003;27:385–93.
[107] Tse SD, Zhu DL, Law CK. Morphology and burning rates of expanding spherical flames in H-2/O-2/inert mixtures up to 60 atm. In: Proceedings of the combustion institute, vol. 28; 2000. p. 1793–800.
[108] Qiao L, Kim CH, Faeth GM. Suppression effects of diluents on laminar premixed hydrogen/oxygen/nitrogen flames. Combust Flame 2005;143: 79–96.
[109] Dahoe AE. Laminar burning velocities of hydrogen–air mixtures from closed vessel gas explosions. J Loss Prev Process Ind 2005;18:152–66.
[110] Hermanns RTE, Konnov AA, Bastiaans RJM, de Goey LPH. Laminar burning velocities of diluted hydrogen–oxygen–nitrogen mixtures. Energy Fuels 2007;21:1977–81.
[111] Botha JP, Spalding DB. The laminar flame speed of propane/air mixtures with heat extraction from the flame. Proc R Soc Lond Ser: Math Phys Sci 1954;225:71–96.
[112] Davis SG, Law CK. Determination of and fuel structure effects on laminar flame speeds of C1 to C8 hydrocarbons. Combust Sci Technol 1998;140: 427–49.
[113] Dong Y, Vagelopoulos CM, Spedding GR, Egolfopoulos FN. Measurement of laminar flame speeds through digital particle image velocimetry: mixtures of methane and ethane with hydrogen, oxygen, nitrogen, and helium. In: Proceedings of the combustion institute, vol. 29; 2002. p. 1419–26.
[114] Johnston RJ, Farrell JT. Laminar burning velocities and Markstein lengths of aromatics at elevated temperature and pressure. In: Proceedings of the combustion institute, vol. 30; 2005. p. 217–24.
[115] Liao SY, Jiang DM, Gao J, Huang ZH, Cheng Q. Measurements of Markstein numbers and laminar burning velocities for liquefied petroleum gas–air mixtures. Fuel 2004;83:1281–8.
[116] Vagelopoulos CM, Egolfopoulos FN. Direct experimental determination of laminar flame speeds. In: Symposium (international) on combustion, vol. 27; 1998. p. 513–9.
[117] Vagelopoulos CM, Egolfopoulos FN, Law CK. Further considerations on the determination of laminar flame speeds with the counterflow twin-flame

technique. In: Symposium (international) on combustion, vol. 25; 1994. p. 1341–7.
[118] Zhao Z, Kazakov A, Dryer FL. Measurements of dimethyl ether/air mixture burning velocities by using particle image velocimetry. Combust Flame 2004;139:52–60.
[119] Bradley D, Gaskell PH, Gu XJ. Burning velocities, Markstein lengths, and flame quenching for spherical methane–air flames: a computational study. Combust Flame 1996;104:176–98.
[120] Gu XJ, Haq MZ, Lawes M, Woolley R. Laminar burning velocity and Markstein lengths of methane–air mixtures. Combust Flame 2000;121:41–58.
[121] Konnov AA, Dyakov IV, De Ruyck J. Measurement of adiabatic burning velocity in ethane–oxygen–nitrogen and in ethane–oxygen–argon mixtures. Exp Thermal Fluid Sci 2003;27:379–84.
[122] Marley SK, Roberts WL. Measurements of laminar burning velocity and Markstein number using high-speed chemiluminescence imaging. Combust Flame 2005;141:473–7.
[123] Metghalchi M, Keck JC. Laminar burning velocity of propane–air mixtures at high temperature and pressure. Combust Flame 1980;38:143–54.
[124] Zhou M, Garner CP. Direct measurements of burning velocity of propane–air using particle image velocimetry. Combust Flame 1996;106:363–7.
[125] Rozenchan G, Zhu DL, Law CK, Tse SD. Outward propagation, burning velocities, and chemical effects of methane flames up to 60 ATM. In: Proceedings of the combustion institute, vol. 29; 2002. p. 1461–70.
[126] Di Sarli V, Benedetto AD. Laminar burning velocity of hydrogen–methane/air premixed flames. Int J Hydrog Energy 2007;32:637–46.
[127] Hu E, Huang Z, He J, Jin C, Zheng J. Experimental and numerical study on laminar burning characteristics of premixed methane–hydrogen–air flames. Int J Hydrog Energy 2009;34:4876–88.
[128] Law CK, Kwon OC. Effects of hydrocarbon substitution on atmospheric hydrogen–air flame propagation. Int J Hydrog Energy 2004;29:867–79.
[129] Briones AM, Aggarwal SK, Katta VR. Effects of H2 enrichment on the propagation characteristics of CH4–air triple flames. Combust Flame 2008;153:367–83.
[130] Choudhuri AR, Gollahalli SR. Combustion characteristics of hydrogen–hydrocarbon hybrid fuels. Int J Hydrog Energy 2000;25:451–62.
[131] Hu E, Huang Z, He J, Zheng J, Miao H. Measurements of laminar burning velocities and onset of cellular instabilities of methane–hydrogen–air flames at elevated pressures and temperatures. Int J Hydrog Energy 2009;34:5574–84.
[132] Wang J, Huang Z, Tang C, Miao H, Wang X. Numerical study of the effect of hydrogen addition on methane–air mixtures combustion. Int J Hydrog Energy 2009;34:1084–96.
[133] Hu E, Huang Z, Liu B, Zheng J, Gu X, Huang B. Experimental investigation on performance and emissions of a spark-ignition engine fuelled with natural gas–hydrogen blends combined with EGR. Int J Hydrog Energy 2009;34:528–39.
[134] Wang H, X.You, Joshi AV, Davis SG, Laskin A, Egolfopoulos F, et al. High-temperature combustion reaction model of H2/CO/C1–C4 compounds. USC Mech Version II; May 2007. 〈http://ignis.usc.edu/USC_Mech_II.htm〉.
[135] Law CK, Jomaas G, Bechtold JK. Cellular instabilities of expanding hydrogen/propane spherical flames at elevated pressures: theory and experiment. In: Proceedings of the combustion institute, vol. 30; 2005. p. 159–67.
[136] Qin Z, Lissianski VV, Yang H, Gardiner WC, Davis SG, Wang H. Combustion chemistry of propane: a case study of detailed reaction mechanism optimization. In: Symposium (international) on combustion, vol. 28; 2000. p. 1663–9.
[137] Law CK, Sung CJ. Structure, aerodynamics, and geometry of premixed flamelets. Prog Energy Combust Sci 2000;26:459–505.
[138] Sun CJ, Sung CJ, He L, Law CK. Dynamics of weakly stretched flames: quantitative description and extraction of global flame parameters. Combust Flame 1999;118:108–28.
[139] Egolfopoulos FN, Law CK. Chain mechanisms in the overall reaction orders in laminar flame propagation. Combust Flame 1990;80:7–16.
[140] Mandilas C, Ormsby MP, Sheppard CGW, Woolley R. Effects of hydrogen addition on laminar and turbulent premixed methane and *iso*-octane–air flames. In: Proceedings of the combustion institute, vol. 31; 2007. p. 1443–50.
[141] Sher E, Ozdor N. Laminar burning velocities of *n*-butane/air mixtures enriched with hydrogen. Combust Flame 1992;89:214–20.
[142] Bradley D, Sheppart CGW, Woolley R, Greenhalgh DA, Lockett RD. The development and structure of flame instabilities and cellularity at low Markstein numbers in explosions. Combust Flame 2000;122:195–209.
[143] Groff EG. The cellular nature of confined spherical propane–air flames. Combust Flame 1982;48:51–62.
[144] Liberman MA, Bychkov VV, Golberg SM, Eriksson LE. Numerical study of curved flames under confinement. Combust Sci Technol 1998;136:221–51.
[145] Liberman MA, Ivanov MF, Peil OE, Valiev DM, Eriksson LE. Numerical modeling of the propagating flame and knock occurrence in spark-ignition engines. Combust Sci Technol 2005;177:151–82.
[146] Darrieus G. Propagation d'un front de flame, unpublished work presented at Paris, in La Technique Moderne and le Congrès de Méchanique Appliquée; 1938.
[147] Landau LD. On the theory of slow combustion. Acta Physicochim, URSS 1944;19:77–88.
[148] Markstein GH. Cell structure of propane flames burning in tubes. J Chem Phys 1949;17:428–9.
[149] Sivashinsky GI. Instabilities, pattern formation, and turbulence in flames. Annu Rev Fluid Mech 1983;15:179.
[150] Kadowaki S. The body-force effect on the cell formation of premixed flames. Combust Flame 2001;124:409–21.
[151] Clanet C, Searby G. First experimental study of the Darrieus–Landau instability. Phys Rev Lett 1998;80:3867.
[152] Bechtold JK, Matalon M. Hydrodynamic and diffusion effects on the stability of spherically expanding flames. Combust Flame 1987;67:77–90.
[153] Parlange JY. Influence of preferential diffusion on the stability of a laminar flame. J Chem Phys 1968;48:1843–9.
[154] Jomaas G, Law CK, Bechtold JK. On transition to cellularity in expanding spherical flames. J Fluid Mech 2007;583:1–26.
[155] Tang CL, Huang ZH, Wang JH, Zheng JJ. Effects of hydrogen addition an cellular instabilities of the spherically expanding propane flames. Int J Hydrog Energy 2009;34:2483–7.
[156] Ren JY, Qin W, Egolfopoulos FN, Tsotsis TT. Strain-rate effects on hydrogen-enhanced lean premixed combustion. Combust Flame 2001;124:717–20.
[157] Schefer RW. Hydrogen enrichment for improved lean flame stability. Int J Hydrog Energy 2003;28:1131–41.
[158] Schefer RW, Wicksall DM, Agrawal AK. Combustion of hydrogen-enriched methane in a lean premixed swirl-stabilized burner. In: Proceedings of the combustion institute, vol. 29; 2002. p. 843–51.
[159] Strakey P, Sidwell T, Ontko J. Investigation of the effects of hydrogen addition on lean extinction in a swirl stabilized combustor. In: Proceedings of the combustion institute, vol. 31; 2007. p. 3173–80.
[160] Jackson GS, Sai R, Plaia JM, Boggs CM, Kiger KT. Influence of H2 on the response of lean premixed CH4 flames to high strained flows. Combust Flame 2003;132:503–11.